2. Materials and methods

2.1. Animals

The study was reviewed and approved by the Committee on Ethics of Animal Experiments, Kyushu University Graduate School of Medical Sciences, and was conducted according to the Guidelines for Animal Experiments of Kyushu University. Male Institute of Cancer Research (ICR) mice (8–10 weeks old; SLC, Fukuoka, Japan) were used.

2.2. Mouse heart failure model preparation

The mice underwent LCA occlusion to produce MI (MI group). The surgical procedures are described in detail elsewhere (Michael et al., 1995). Briefly, after sodium pentobarbital anaesthesia (25–40 mg/kg intraperitoneally) and intubation with a polyethylene tube, the animals were ventilated using a volume-cycled rodent respirator with a 2–3 mL/cycle and at a respiratory rate of 120 breaths/min. After thoracotomy, the LCA was ligated with a suture 3–4 mm from the tip of the left auricle. The chest wall and skin were then closed with sutures. A sham operation (without LCA occlusion) was similarly performed on the control group (sham-operated group).

The resultant infarcts were evaluated using serial 5-μm sections stained with Masson's trichrome stain. Infarct length was measured along the endocardial and epicardial surfaces from the LV sections. Total LV circumference was calculated as the sum of endocardial and epicardial segment lengths. Infarct size was calculated as the infract circumference divided by the total circumference times 100.

2.3. Echocardiographic imaging

Just before and ten days after LCA occlusion, serial M-mode echocardiographies were performed on all animals under light sodium pentobarbital anaesthesia with spontaneous respiration. An echocardiography system (SSD5000; Aloka, Tokyo, Japan) with a dynamically focused 7.5-MHz linear array transducer was used. M-mode tracings were recorded from the short-axis view at the level of the papillary muscle. LV end-diastolic diameter (LVEDD), LV end-systolic diameter (LVESD) and wall thickness were measured. Percent fractional shortening (%FS) was calculated as follows: %FS = (LVEDD) − (LVESD)/(LVEDD) × 100.

2.4. Continuous intracisternal infusion with a Rho-kinase inhibitor

Two days before LCA occlusion, the mice were anaesthetized with sodium pentobarbital (50 mg/kg intraperitoneally). An osmotic minipump – filled with a vehicle (artificial cerebrospinal fluid containing 123 mM NaCl, 0.86 mM $CaCl_2$, 3.0 mM KCl, 0.89 mM $MgCl_2$, 25 mM $NaHCO_3$, 0.5 mM NaH_2PO_4 and 0.25 mM Na_2HPO_4; pH 7.4) or with Y-27632 dissolved in artificial cerebrospinal fluid – was subcutaneously implanted in the dorsum of each of the mice and connected to a polyethylene tube (PE-10). The osmotic mini-pump infusion rate was 0.25 μL/h and the pumps were calibrated to empty after 14 days. A small hole was made in the atlantooccipital membrane, which covers the dorsal surface of the medulla, and the tip of the tube was placed intracisternally and fixed in place with tissue adhesive.

2.5. Measurement of blood pressure and heart rate

At day 10 after the interventions (LCA occlusion and sham operation), the systolic blood pressure and heart rate were measured using the tail-cuff method in an awake state.

2.6. Evaluation of Rho-kinase activity

At day 10 after the interventions (LCA occlusion and sham operation), the animals were sacrificed using an overdose of sodium pentobarbital and brainstem tissues were obtained. The tissues were homogenized in a lysing buffer containing 40 mmol/L HEPES (4-[2-hydroxyethyl]-1-piperazineethanesulfonic acid), 1% Triton® X-100, 10% glycerol, 1 mmol/L Na_3VO_4 (sodium orthovanadate) and 1 mmol/L phenylmethylsulfonyl fluoride. The tissue lysate was centrifuged and the supernatant collected. The protein concentration was determined using a BCA (bicinchoninic acid) protein assay kit (Pierce Chemical Co., Rockford, IL). An aliquot part of 15 μg of protein from each sample was separated on 10% sodium dodecyl sulfate–polyacrylamide gel. The proteins were subsequently transferred onto polyvinylidene difluoride (PVDF) membranes (Immobilon®-P membrane; Millipore, Billerica, MA). Membranes were incubated with goat immunoglobin G (IgG) monoclonal antibody to Rho-kinase (ROCK-2; 1:1000, Santa Cruz Biotechnology, CA), with rabbit IgG polyclonal antibody to RhoA (1:1000, Santa Cruz Biotechnology) or with rabbit anti-phosphorylated ERM family members – ezrin (Thr567), radixin (Thr564) and moesin (Thr558) – which are target proteins of Rho-kinase (Matsui et al., 1998). Membranes were then incubated with a horseradish peroxidase-conjugated horse anti-goat or rabbit IgG antibody (1:10,000). Rabbit IgG polyclonal antibody to β-tubulin (1:5000, Santa Cruz Biotechnology) for the brain tissues was used as an internal control. Immunoreactivity was detected by enhanced chemiluminescence autoradiography (ECL™ Western blotting detection kit; Amersham Pharmacia Biotech, Uppsala, Sweden), and the film was analyzed using NIH Image.

2.7. Measurement of organ weight

When the mice were sacrificed, the liver and lungs were also removed and weighed.

2.8. Measurement of urinary norepinephrine excretion

The 24-hour urinary norepinephrine (U-NE) excretion was measured by high-performance liquid chromatography two days before and nine days after LCA occlusion.

2.9. Statistics

All values are expressed as mean ± S.E. An unpaired *t*-test was used to compare values between the MI mice and sham-operated mice. A paired *t*-test was used to compare the values before and after each operation in the sham-operated mice and MI mice. A two-way ANOVA was used to compare the LVEDD and %FS between the MI group infused with the vehicle (MI + vehicle group) and the MI group infused with Y-27632 (MI + Y-27632 group). Differences were considered to be significant when $P < 0.05$.

3. Results

3.1. Heart failure characteristics

Systolic blood pressure and heart rate did not significantly alter after MI. The weight of the liver and lungs significantly increased in

Table 1
Physiological parameters of each group

	Sham ($n=10$)	MI + vehicle ($n=9$)	MI + Y-27632 ($n=10$)
Body weight (g)	43 ± 3	40 ± 5	39 ± 4
Lung (mg)/BW(g)	5.7 ± 0.1	7.2 ± 0.2*	6.8 ± 0.2*
Liver (mg)/BW(g)	6.8 ± 0.7	8.8 ± 0.4*	7.7 ± 0.3*
Heart (mg)/BW(g)	3.6 ± 0.1	4.0 ± 0.4	3.9 ± 0.3
SBP (mm Hg)	124 ± 15	126 ± 12	118 ± 11
HR (bpm)	422 ± 33	442 ± 28	398 ± 30

Values are means ± S.E; *n*, number of mice.
* $P < 0.05$ versus sham group.

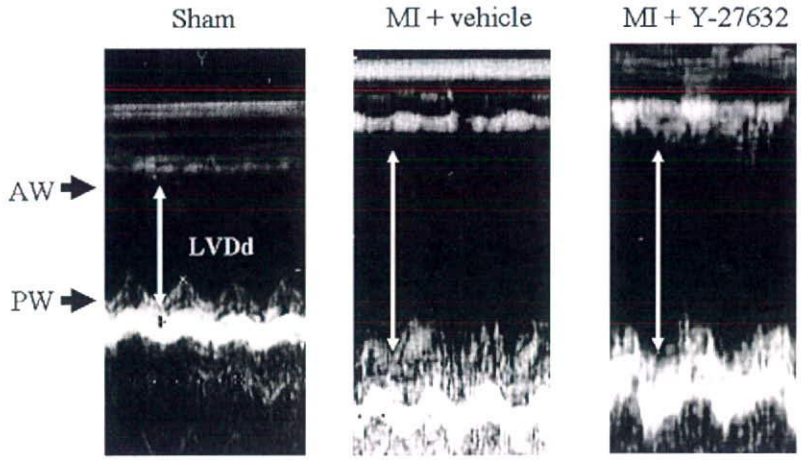

Fig. 1. M-mode echocardiograms of the left ventricle in parasternal short-axis view obtained from the sham-operated group, the myocardial infarction group with the vehicle (MI+vehicle) and the myocardial infarction group with Y-27632 (MI+Y-27632). LVEDd: left ventricular end-diastolic diameter; AW: anterior wall; PW: posterior wall.

the MI group compared with the sham-operated group (Table 1). Infarct size did not differ between the MI+vehicle group and MI+Y-27632 group (55±3% versus 55±2%). Echocardiographic evaluation revealed that the LVEDD was larger and %FS was smaller in the MI group than in the sham-operated group (Fig. 1, Table 2). Furthermore, the 24-hour U-NE excretion was significantly higher in the MI group compared with the sham-operated group (Fig. 2).

3.2. Effects of Rho-kinase inhibition in the brainstem on heart failure characteristics

Intracisternal infusion of Rho-kinase inhibitor Y-27632 significantly attenuated the increases in 24-hour U-NE excretion in the MI group to levels similar to those of before the LCA occlusion, indicating that intracisternal infusion of Y-27632 prevented the increase in sympathetic nerve activation in the MI group (Fig. 2). The echocardiographic values and organ weights did not differ statistically between the MI+Y-27632 group and MI+vehicle group (Tables 1 and 2). Although systolic blood pressure and heart rate also did not significantly differ between the MI+vehicle group and MI+Y-27632 group, heart rate tended to decrease in the MI+Y-27632 group compared with the MI+vehicle group ($p=0.1$; Table 1).

In the sham-operated group ($n=4$), Y-27632 did not affect the systolic blood pressure (125±11 mm Hg), heart rate (414±20 bpm) or U-NE excretion (Fig. 2).

3.3. RhoA and Rho-kinase protein expression and Rho-kinase activity in brainstem

The levels of RhoA and Rho-kinase proteins did not change in any group (Fig. 3). However, the levels of phosphorylated ezrin/radixin/moesin (p-ERM) proteins, which indicate Rho-kinase activity, were higher in the MI group compared with the sham-operated group (Fig. 3). Intracisternal infusion of Y-27632 significantly attenuated the expression level of p-ERM proteins in the MI group to levels similar to those of the sham-operated group (Fig. 3).

Table 2
Echocardiographic parameters of each group

	Sham ($n=10$)	MI+vehicle ($n=9$)	MI+Y-27632 ($n=10$)
LVDd (mm)	3.4±0.3	4.1±0.1*	3.8±0.5*
LVDs (mm)	2.1±0.1	2.5±0.1*	2.2±0.4*
FS (%)	39±2	17±1*	18±1*

Value are means±S.E; *n*, number of mice; LVEDD, left ventricular end-diastolic dimension; LVESD, left ventricular end-systolic dimension; %FS, percent fractional shortening.
* $P<0.05$ versus sham group.

4. Discussion

The major finding in this study was that the Rho/Rho-kinase pathway in the brainstem contributes to the activation of the sympathetic nervous system in mice with heart failure after MI. U-NE and Rho-kinase activity were increased in the brainstem of these mice. Inhibition of Rho-kinase activity in the brainstem by intracisternal infusion of Y-27632 significantly reduced U-NE. These findings suggest that increased Rho-kinase activity in the brainstem contributes to the sympathetic hyperactivation in mice with heart failure after MI.

In the mice, heart failure was produced by LCA occlusion. The resulting LV dilatation and reduced LV systolic function were confirmed by echocardiography. Also, U-NE, a marker of sympathetic nerve activity, was significantly increased in the MI mice. Heart failure is characterized by an enhanced sympathetic drive in experimental animals as well as in patients (Mark, 1995; Zucker et al., 1995; Middlekauff and Mark, 1998). In patients with heart failure, plasma norepinephrine levels increase with the severity of heart failure. Furthermore, in heart failure, the weight of the lungs and liver increases due to congestion. In this study, we confirmed that the weight of the lungs and liver significantly increased in the MI mice

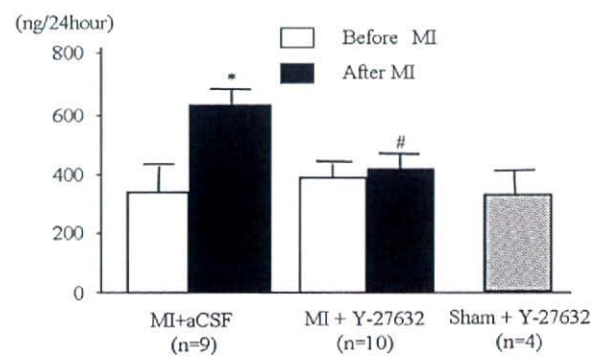

Fig. 2. The 24-hour urinary norepinephrine (U-NE) excretion in each group (*$P<0.05$ versus before myocardial infarction [MI], #$P<0.05$ versus myocardial infarction group with the vehicle [MI+vehicle]).

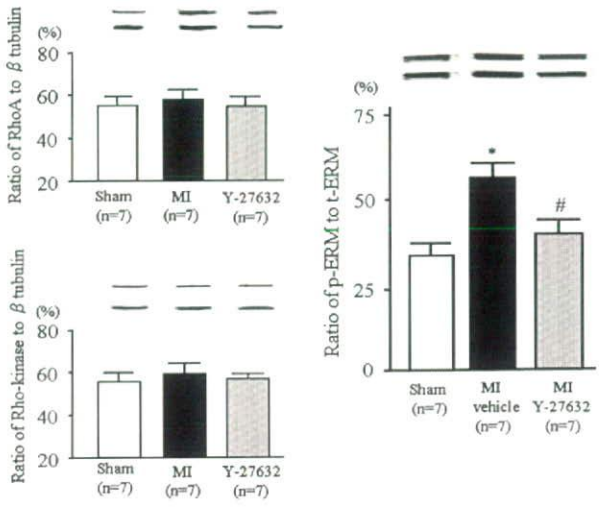

Fig. 3. Left: Level of RhoA and Rho-kinase protein in the brainstem in each group. Right: Level of phosphorylated ezrin/radixin/moesin (p-ERM) family, a target protein of Rho-kinase, in the brainstem in each group (*$P<0.05$ versus sham-operated group, #$P<0.05$ versus myocardial infarction group with the vehicle [MI+vehicle]).

compared with the sham-operated mice. These results indicate that the MI mice were in a heart failure state, validating the use of these mice as a heart failure model.

In recent studies, we had demonstrated that the Rho/Rho-kinase pathway in the brainstem is involved in blood pressure regulation and baroreflex function via the sympathetic nervous system, and activation of this pathway contributes to the central hypertensive mechanisms of several hypertensive models (Ito et al., 2003, 2004a, 2005a,b, 2006). The Rho/Rho-kinase pathway is activated by angiotensin II (Sagara et al., 2007; Funakoshi et al., 2001), and angiotensin II may have an important role in sympathetic nerve activation of heart failure (Felder et al., 2001; Shigematsu et al., 2001; Zucker, 2006). Further, an increase in angiotensin II may be necessary for sustained sympathetic hyperactivation in heart failure (Liu and Zucker, 1999). Inhibition of angiotensin II type1 receptors in the NTS reduces blood pressure, heart rate, and sympathetic nerve activity in rats with chronic inhibition of nitric oxide synthase (Eshima et al., 2000). Therefore, we hypothesized that the Rho/Rho-kinase pathway in the brainstem contributes to sympathetic nerve activation in mice with heart failure after MI, and we evaluated the role of this pathway in the brainstem in sympathetic hyperactivation.

The finding that the increase in U-NE in the MI mice was significantly reduced by an intracisternal infusion of Y-27632 was most important in this study, and this finding indicates that the Rho/Rho-kinase pathway in the brainstem contributes to the increase in sympathetic nerve activity after MI. We evaluated sympathetic nerve activity by the U-NE, which may be dependent on renal function. Although we did not assess this issue, the criterion of using U-NE for the estimation of sympathetic nerve activity in heart failure models has already been established (Sakai et al., 2005). Furthermore, the aim of our study was to compare the effects of Rho-kinase inhibition on the sympathetic nerve activity between the MI+Y-27632 group and MI+vehicle group. Therefore, we measured the U-NE excretion as a marker of sympathetic nerve activity.

The mechanisms of blood pressure regulation by Rho-kinase have not been fully understood. Inhibition of Rho-kinase enhances glutamate sensitivity in excitatory synapses, such as in the NTS (Ito et al., 2005a). Whether this mechanism contributed to the reduced sympathetic nerve activity caused by Y-27632 in the MI mice remains unknown. A study has reported that the Rho/Rho-kinase pathway negatively regulates endothelial nitric oxide synthase (NOS) expression (Laufs and Liao, 1998). Also, nitric oxide in the brain inhibits sympathetic nerve activity (Sakai et al., 2000; Kishi et al., 2001, 2002). In fact, a recent study demonstrated that NOS expression in the brainstem, especially in the NTS, is reduced in an MI mouse model of heart failure, and up-regulation of NOS in the NTS attenuates the enhanced sympathetic drive (Sakai et al., 2005). Therefore, attenuation of the sympathetic drive by intracisternal infusion of Y-27632 might be by an effect of nitric oxide.

We evaluated the Rho-kinase activity using the p-ERM levels as one of the markers. Other target proteins, such as adducin and cofilin, might also have been phosphorylated by Rho-kinase, and the levels of these proteins could have changed. In fact, in an earlier study, we had demonstrated that phosphorylated adducin (p-adducin) levels also increased in the brainstem of spontaneously hypertensive rats compared with Wistar–Kyoto rats (Ito et al., 2003).

As seen from the results of earlier studies (Funakoshi et al., 2001; Matsumoto et al., 2008), factors such as angiotensin II and endothelin also play a role in activating the Rho/Rho-kinase pathway. Also, in previous studies, we had reported that central angiotension II produced pressor responses by the activation of Rho-kinase in the brainstem (Sagara et al., 2007), and that in the heart failure model, the renin–angiotensin system (RAS) was activated in the brainstem (Shigematsu et al., 2001). Therefore, RAS might be one of the mechanisms for Rho-kinase stimulation in heart failure. However, we have not addressed these issues in this study. Further research is needed to confirm these hypotheses.

5. Study limitations

Intracisternal infusion of Y-27632 might affect many areas of the brain, including the cardiovascular centre, and it is not possible to identify specific areas affected by intracisternally infused drugs. Intracisternal infusion of Y-27632 might also alter neuronal activity in areas other than in the NTS, such as in the RVLM, due to the flow of cerebrospinal fluid. Therefore, we examined Rho-kinase activity in the whole brainstem for this study. As we had previously demonstrated that Y-27632 has greater effects on blood pressure when injected into the NTS rather than into the RVLM of rats (Ito et al., 2005b), we speculate that intracisternal infusion of Y-27632 alters neuronal activity mainly in the NTS. However, we could not confirm this speculation because of the technical difficulties involved in using mice as experimental animals.

In this study, we did not find an improvement in cardiac function despite the attenuation of sympathetic nerve activation by the Rho-kinase inhibitor. These results might be attributed to the brief treatment and survey duration. In fact, LV dimensions tended to decrease in the MI+Y-27632 group rather than in the MI+vehicle group. Thus, if we had treated the MI group with Y-27632 for a much longer period, it might have been possible to detect a significant improvement in cardiac function. Therefore, further study is needed to evaluate the long-term effects of Rho-kinase inhibition on improvement of cardiac function or on survival.

6. Conclusion

After MI, the mice showed characteristics consistent with those of heart failure. From the enhanced sympathetic nerve activity observed, it can be concluded that this enhancement is mediated by Rho-kinase in the brainstem. In addition, treatment with a Rho-kinase inhibitor before LCA occlusion might have preventive effects on heart failure deterioration.

Acknowledgements

This study was supported by Grants-in-Aid for Scientific Research from the Japan Society for the Promotion of Science.

References

Benedict, C.R., Shelton, B., Johnstone, D.E., Francis, G., Greenberg, B., Konstam, M., Probstfield, J.L., Yusuf, S., 1996. Prognostic significance of plasma norepinephrine in patients with asymptomatic left ventricular dysfunction. Circulation 94, 690–697.

Bristow, M.R., O'Connell, J.B., Gilbert, E.M., French, W.J., Leathermen, G., Kantrowitz, N.E., Orie, J., Smucker, M.L., Marshall, G., Kelly, P., 1994. Dose-response of chronic beta-blocker treatment in heart failure from either idiopathic dilated or ischemic cardiomyopathy. Circulation 89, 1632–1642.

Cohn, J.N., Levine, T.B., Olivari, M.T., Garberg, V., Lura, D., Francis, G.S., Simon, A.B., Rector, T., 1984. Plasma norepinephrine as a guide to prognosis in patients with chronic congestive heart failure. N. Engl. J. Med. 311, 819–823.

Dampney, R.A.L., Polson, J.W., Potts, P.D., Hirooka, Y., 1994. Functional organization of central pathway regulating the cardiovascular system. Physiol. Rev. 74, 323–364.

Eshima, K., Hirooka, Y., Shigematsu, H., Matsuo, I., Koike, G., Sakai, K., Takeshita, A., 2000. Angiotensin II in the nucleus tractus solitarii contributes to neurogenic hypertension caused by chronic nitric oxide synthase inhibition. Hypertension 36, 259–263.

Felder, R.B., Francis, J., Weiss, R.M., Zhang, Z.H., Wei, S.G., Johnson, A.K., 2001. Neurohumoral regulation in ischemia-induced heart failure. Role of the forebrain. Ann. N.Y. Acad. Sci. 940, 444–453.

Francis, G.S., Benedict, C., Johnstone, D.E., Kirlin, P.C., Nicklas, J., Liang, C.S., Kubo, S.H., Rudin-Toretsky, E., Yusuf, S., 1990. Comparison of neuroendocrine activation in patients with left ventricular dysfunction with and without congestive heart failure. A substudy of the Studies of Left Ventricular Dysfunction (SOLVD). Circulation 82, 1724–1729.

Funakoshi, Y., Ichiki, T., Shimokawa, H., Egashira, K., Takeda, K., Kaibuchi, K., Takeya, M., Yoshimura, T., Takeshita, A., 2001. A critical role of Rho-kinase in angiotensin II-induced monocyte chemoattractant protein-1 expression in rat vascular smooth muscle cells. Hypertension 38, 100–104.

Ito, K., Hirooka, Y., Sakai, K., Kishi, T., Kaibuchi, K., Shimokawa, H., Takeshita, A., 2003. Rho/Rho-kinase pathway in brainstem contributes to blood pressure regulation via sympathetic nervous system; possible involvement in neural mechanisms of hypertension. Circ. Res. 92, 1337–1343.

Ito, K., Hirooka, Y., Kishi, T., Kimura, Y., Kaibuchi, K., Shimokawa, H., Takeshita, A., 2004a. Rho/Rho-kinase pathway in the brainstem contributes to hypertension caused by chronic nitric oxide synthase inhibition. Hypertension 43, 156–162.

Ito, K., Hirooka, Y., Sagara, Y., Kimura, Y., Kaibuchi, K., Shimokawa, H., Takeshita, A., Sunagawa, K., 2004b. Inhibition of Rho-kinase in the brainstem augments baroreflex control of heart rate in rats. Hypertension 44, 478–483.

Ito, K., Hirooka, Y., Hori, N., Kimura, Y., Sagara, Y., Shimokawa, H., Takeshita, A., Sunagawa, K., 2005a. Inhibition of Rho-kinase in the nucleus tractus solitarius enhances glutamate sensitivity in rats. Hypertension 46, 360–365.

Ito, K., Hirooka, Y., Kimura, Y., Shimokawa, H., Takeshita, A., 2005b. Effects of hydroxyfasudil administered to the nucleus tractus solitarii on blood pressure and heart rate in spontaneously hypertensive rats. Clin. Exp. Hypertens. 2, 269–277.

Ito, K., Hirooka, Y., Kimura, Y., Sagara, Y., Sunagawa, K., 2006. Ovariectomy augments hypertension through Rho-kinase activation in the brain stem in female spontaneously hypertensive rats. Hypertension 48, 651–657.

Kishi, T., Hirooka, Y., Sakai, K., Shigematsu, H., Shimokawa, H., Takeshita, A., 2001. Overexpression of eNOS in the RVLM causes hypotension and bradycardia via GABA release. Hypertension 38, 896–901.

Kishi, T., Hirooka, Y., Ito, K., Sakai, K., Shimokawa, H., Takeshita, A., 2002. Cardiovascular effects of overexpression of endothelial nitric oxide synthase in the rostral ventrolateral medulla in stroke-prone spontaneously hypertensive rats. Hypertension 39, 264–268.

Laufs, U., Liao, J.K., 1998. Post-transcriptional regulation of endothelial nitric oxide synthase mRNA stability by Rho GTPase. J. Biol. Chem. 273, 24266–24271.

Liu, J.L., Zucker, I.H., 1999. Regulation of sympathetic nerve activity in heart failure: a role for nitric oxide and angiotensin II. Circ. Res. 94, 402–423.

Mark, A.L., 1995. Sympathetic dysregulation in heart failure: mechanisms and therapy. Clin. Cardiol. 18, I3–I8.

Matsui, T., Maeda, M., Doi, Y., Yonemura, S., Amano, M., Kaibuchi, K., Tsukita, S., 1998. Rho-kinase phosphorylates COOH-terminal threonines of ezrin/radixin/moesin (ERM) proteins and regulates their head-to-tail association. J. Cell Biol. 140, 647–657.

Matsumoto, T., Kakami, M., Kobayashi, T., Kamata, K., 2008. Gender differences in vascular reactivity to endothelin-1 (1-31) in mesenteric arteries from diabetic mice. Peptides 29, 1338–1346.

Michael, L.H., Entman, M.L., Hartley, C.J., Youler, K.A., Zhu, J., Hall, S.R., Hawkins, H.K., Berens, K., Ballantyne, C.M., 1995. Myocardial ischemia and reperfusion: a murine model. Am. J. Physiol. 269, H2147–H2154.

Middlekauff, H.R., Mark, A.L., 1998. The treatment of heart failure: the role of neurohumoral activation. Intern. Med. 37, 112–122.

Packer, M., Bristow, M.R., Cohn, J.N., Colucci, W.S., Fowler, M.B., Gilbert, E.M., Shusterman, N.H., 1996. The effect of carvedilol on morbidity and mortality in patients with chronic heart failure. U.S. Carvedilol Heart Failure Study Group. N. Engl. J. Med. 334, 1349–1355.

Rector, T.S., Olivari, M.T., Levine, T.B., Francis, G.S., Cohn, J.N., 1987. Predicting survival for an individual with congestive heart failure using the plasma norepinephrine concentration. Am. Heart J. 114, 148–152.

Sagara, Y., Hirooka, Y., Nozoe, M., Ito, K., Kimura, Y., Sunagawa, K., 2007. Pressor responses induced by central angiotensin II is mediated by activation of Rho/Rho-kinase pathway via AT1 receptors. J. Hypertens. 25, 399–406.

Sakai, K., Hirooka, Y., Matsuo, I., Eshima, K., Shigematsu, H., Shimokawa, H., Takeshita, A., 2000. Overexpression of eNOS in NTS causes hypotension and bradycardia in vivo. Hypertension 36, 1023–1028.

Sakai, K., Hirooka, Y., Shigematsu, H., Kishi, T., Ito, K., Shimokawa, H., Takeshita, A., Sunagawa, K., 2005. Overexpression of eNOS in brain stem reduces enhanced sympathetic drive in mice with myocardial infarction. Am. J. Physiol. Heart Circ. Physiol. 289, H2159–H2166.

Shigematsu, H., Hirooka, Y., Eshima, K., Shihara, M., Tagawa, T., Takeshita, A., 2001. Endogenous angiotensin II in the NTS contributes to sympathetic activation in rats with aortocaval shunt. Am. J. Physiol. 280, 1665–1673.

Waagstein, F., Bristow, M.R., Swedberg, K., Camerini, F., Fowler, M.B., Silver, M.A., Gilbert, E.M., Johnson, M.R., Goss, F.G., Hjalmarson, A., 1993. Beneficial effects of metoprolol in idiopathic dilated cardiomyopathy. Metoprolol in Dilated Cardiomyopathy (MDC) Trial Study Group. Lancet 342, 1441–1446.

Zucker, I.H., 2006. Novel mechanisms of sympathetic regulation in chronic heart failure. Hypertension 48, 1005–1011.

Zucker, I.H., Wang, W., Brandle, M., Schultz, H.D., Patel, K.P., 1995. Neural regulation of sympathetic nerve activity in heart failure. Prog. Cardiovasc. Dis. 37, 397–414.

Am J Physiol Heart Circ Physiol 295: H1855–H1866, 2008.
First published August 29, 2008; doi:10.1152/ajpheart.522.2008.

Contrasting effects of presynaptic α_2-adrenergic autoinhibition and pharmacologic augmentation of presynaptic inhibition on sympathetic heart rate control

Tadayoshi Miyamoto,[1,2] Toru Kawada,[2] Yusuke Yanagiya,[2] Tsuyoshi Akiyama,[3] Atsunori Kamiya,[2] Masaki Mizuno,[2] Hiroshi Takaki,[2] Kenji Sunagawa,[4] and Masaru Sugimachi[2]

[1]Department of Physical Therapy, Faculty of Health Sciences, Morinomiya University of Medical Sciences; and [2]Department of Cardiovascular Dynamics, Advanced Medical Engineering Center, and [3]Department of Cardiac Physiology, National Cardiovascular Center Research Institute, Osaka; and [4]Department of Cardiovascular Medicine, Graduate School of Medical Sciences, Kyusyu University, Fukuoka, Japan

Submitted 16 May 2008; accepted in final form 19 August 2008

Miyamoto T, Kawada T, Yanagiya Y, Akiyama T, Kamiya A, Mizuno M, Takaki H, Sunagawa K, Sugimachi M. Contrasting effects of presynaptic α_2-adrenergic autoinhibition and pharmacologic augmentation of presynaptic inhibition on sympathetic heart rate control. *Am J Physiol Heart Circ Physiol* 295: H1855–H1866, 2008. First published August 29, 2008; doi:10.1152/ajpheart.522.2008.—Presynaptic α_2-adrenergic receptors are known to exert feedback inhibition on norepinephrine release from the sympathetic nerve terminals. To elucidate the dynamic characteristics of the inhibition, we stimulated the right cardiac sympathetic nerve according to a binary white noise signal while measuring heart rate (HR) in anesthetized rabbits (n = 6). We estimated the transfer function from cardiac sympathetic nerve stimulation to HR and the corresponding step response of HR, with and without the blockade of presynaptic inhibition by yohimbine (1 mg/kg followed by 0.1 mg·kg^{-1}·h^{-1} iv). We also examined the effect of the α_2-adrenergic receptor agonist clonidine (0.3 and 1.5 mg·kg^{-1}·h^{-1} iv) in different rabbits (n = 5). Yohimbine increased the maximum step response (from 7.2 ± 0.8 to 12.2 ± 1.7 beats/min, means ± SE, $P < 0.05$) without significantly affecting the initial slope (0.93 ± 0.23 vs. 0.94 ± 0.22 beats·min^{-1}·s^{-1}). Higher dose but not lower dose clonidine significantly decreased the maximum step response (from 6.3 ± 0.8 to 6.8 ± 1.0 and 2.8 ± 0.5 beats/min, $P < 0.05$) and also reduced the initial slope (from 0.56 ± 0.07 to 0.51 ± 0.04 and 0.22 ± 0.06 beats·min^{-1}·s^{-1}, $P < 0.05$). Our findings indicate that presynaptic α_2-adrenergic autoinhibition limits the maximum response without significantly compromising the rapidity of effector response. In contrast, pharmacologic augmentation of the presynaptic inhibition not only attenuates the maximum response but also results in a sluggish effector response.

systems analysis; transfer function; α-adrenergic blockade; rabbits

PRESYNAPTIC α_2-ADRENERGIC receptors play an important role in regulating neurotransmitter release in the central and peripheral nervous systems. The concept that neurotransmitter release is modulated by presynaptic autoreceptors was proposed in the 1970s (19, 20, 25, 31–33, 37, 38). Langer (18) first demonstrated that an α-adrenergic antagonist phentolamine, at a concentration below that required to produce its negative chronotropic effect, increases the magnitude of heart rate (HR) response to sympathetic nerve stimulation. Since then, a number of in vivo and in vitro studies have been conducted to characterize the negative feedback regulation of norepinephrine (NE) release via the presynaptic α_2-adrenergic receptors located on the sympathetic nerve terminals (1, 6, 9, 11, 17, 24, 26, 27a, 29, 30, 34, 35). However, the dynamic nature of the presynaptic α_2-adrenergic inhibition in sympathetic HR control remains to be quantified. Because we focus on the effector response to sympathetic nerve stimulation, the term "presynaptic" may be interpreted as "prejunctional" throughout this paper to describe more specifically the NE kinetics at the neuroeffector junction.

We first schematize our hypothesis on the possible modes of operations of the presynaptic inhibition. With reference to Fig. 1, the solid and dotted lines indicate the HR responses with and without the presynaptic inhibition, respectively. Figure 1*A* represents a "limiter-like" operation of the presynaptic inhibition in which the steady-state response is attenuated, while the initial slope of the response is unchanged. Figure 1*B* represents an "attenuator-like" operation in which the steady-state response is attenuated, while the initial slope of the response is also reduced in proportion to the attenuation of the steady-state response. Since the rapid effector response is one of the important hallmarks of neural regulation compared with humoral regulation, determining which of the two operations likely occurs would contribute to the physiological understanding of the presynaptic inhibition. The words "limiter-like" and "attenuator-like" in this paper are used in the specific senses described above.

To answer which of the two operations likely occurs in the presynaptic inhibition, we examined the HR response to dynamic sympathetic nerve stimulation, with or without blocking the α_2-adrenergic receptors in anesthetized rabbits. Because the HR response is mainly mediated by the postsynaptic β_1-adrenergic receptors, the administration of an α_2-adrenergic receptor antagonist does not eliminate the HR response to sympathetic nerve stimulation. We also examined the effects of pharmacologic augmentation of the α_2-adrenergic receptors on the HR response to dynamic sympathetic nerve stimulation. The results of the present study indicated that the presynaptic α_2-adrenergic autoinhibition is a limiter-like operation. In contrast, the pharmacologic

Address for reprint requests and other correspondence: T. Miyamoto, Dept. of Physical Therapy, Faculty of Health Sciences, Morinomiya Univ. of Medical Sciences, Osaka 559-8611, Japan (e-mail: miyamoto@morinomiya-u.ac.jp).

The costs of publication of this article were defrayed in part by the payment of page charges. The article must therefore be hereby marked "*advertisement*" in accordance with 18 U.S.C. Section 1734 solely to indicate this fact.

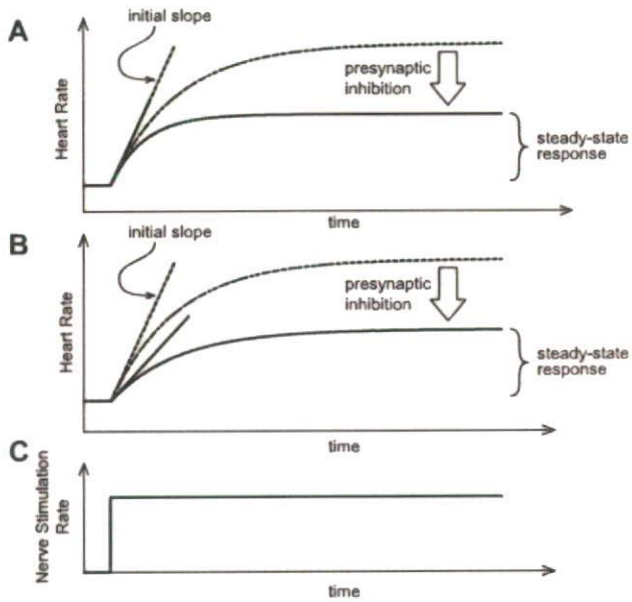

Fig. 1. Schematic representations of the possible operations of the presynaptic inhibition in heart rate (HR) step response to sympathetic nerve stimulation. The solid and dashed lines indicate the HR step response with and without the presynaptic inhibition, respectively. *A*: the presynaptic inhibition attenuates the steady-state response without affecting the initial slope of the response (a "limiter-like" operation). *B*: the presynaptic inhibition attenuates the steady-state response accompanied by a decrease in the initial slope in proportion to the attenuation of the steady-state response (an "attenuator-like" operation). Rapid effector response is maintained in the former but not in the latter. *C*: postulated nerve stimulation rate.

augmentation of presynaptic inhibition is an attenuator-like operation. A possible theoretical explanation for the difference in dynamic characteristics between the presynaptic α_2-adrenergic autoinhibition and the pharmacologic augmentation of the presynaptic inhibition will be proposed.

METHODS

Surgical Preparations

Animal care was in accordance with "Guiding Principles for the Care and Use of Animals in the Field of Physiological Sciences," approved by the Physiological Society of Japan. All protocols were reviewed and approved by the Animal Subject Committee of the National Cardiovascular Center. Japanese white rabbits, weighing 2.5–3.1 kg, were anesthetized by intravenous injection (2 ml/kg) of a mixture of urethane (250 mg/ml) and α-chloralose (40 mg/ml) and mechanically ventilated with oxygen-enriched room air. Tidal volume was set at 35 ml and the rate was adjusted between 35 and 40 cycles/min to be sufficient for suppressing spontaneous respiration. Supplemental doses of these anesthetics were administered by continuous intravenous infusion (1 $ml \cdot kg^{-1} \cdot h^{-1}$) into the marginal ear vein. Arterial pressure (AP) was monitored with a micromanometer catheter (model, Millar Instruments, Houston, TX) inserted into the right femoral artery. A catheter for drug administration was also placed in the right femoral vein. Sinoaortic denervation was performed bilaterally to minimize changes in systemic sympathetic activity via the arterial baroreflexes. The vagi were also sectioned bilaterally at the neck level to remove the vagal control on HR. The right inferior cardiac sympathetic nerve was exposed through a midline thoracotomy and sectioned. A pair of bipolar platinum electrodes was then attached to the cardiac end of the sectioned sympathetic nerve for stimulation (12, 13, 22, 23). The stimulation electrodes and nerve were secured with silicon glue (Kwik-Sil, World Precision Instruments, Sarasota, FL). Instantaneous HR was measured from the AP signal utilizing a cardiotachometer (Tachometer N4778, San-ei, Tokyo, Japan). Body temperature was maintained at 38°C with a heating pad throughout the experiment.

Experimental Procedures

Protocols. To estimate the transfer function from the sympathetic nerve stimulation to HR response, we employed a binary white noise stimulation signal with a switching interval of 5 s. The power spectrum of the sympathetic nerve stimulation rate was fairly constant up to 0.1 Hz and decreased to ~1/10 at 0.15 Hz. The upper frequency limit of the input power that covers the frequency range of physiological interest was determined based on our laboratory's previous studies (12, 23) and also preliminary experimental runs. Different sequences of binary white noise signals were used in different animals. Because HR is linearly related to cardiac output when stroke volume is unchanged, we chose HR as an output signal to understand sympathetic cardiovascular regulation. However, to rule out the possibility that the reciprocal relationship between R-R interval (RRI) and HR confounded the analytical results, we also calculated the transfer function using RRI as an output signal.

In *protocol 1* (n = 6), to examine the dynamic nature of the presynaptic α_2-adrenergic autoinhibition, we estimated the transfer function from dynamic sympathetic nerve stimulation to HR response from 20-min data obtained under control and α_2-adrenergic blockade conditions as follows. After recording the control data, an α_2-adrenergic antagonist yohimbine was administered intravenously with an initial bolus injection of 1 mg/kg, followed by continuous infusion at 0.1 $mg \cdot kg^{-1} \cdot h^{-1}$. The yohimbine bolus was equivalent to 10 h of infusion. The duration from the initiation of yohimbine administration until HR and AP reached new steady-state levels was ~15 min (35). We then repeated the 20-min dynamic sympathetic nerve stimulation and recorded the HR response under the α_2-adrenergic blockade condition.

In *protocol 2* (n = 5), to examine the effects of pharmacologic augmentation of the presynaptic α_2-adrenergic inhibition on the sympathetic HR control, we estimated the transfer function from dynamic sympathetic nerve stimulation to HR response before and during the administration of an α_2-adrenergic receptor agonist clonidine. Clonidine was administered intravenously at 0.3 and 1.5 $mg \cdot kg^{-1} \cdot h^{-1}$ in an increasing order. After 20-min baseline data collection, we started lower dose clonidine administration and waited for 15 min and then collected data for 20 min. Next, we started higher dose clonidine administration and waited for 15 min and then collected data for 20 min.

The stimulation rate of binary white noise was set at 0–1 Hz for *protocol 1*, and 0–5 Hz for *protocol 2*. Because we expected that blockade of the presynaptic α_2-adrenergic inhibition would augment, whereas activation of the inhibition would attenuate, the HR response, we set a higher stimulation rate for *protocol 2* than for *protocol 1*. The pulse width of sympathetic stimulation was set at 2 ms. The amplitude was set so that 5-Hz tonic sympathetic stimulation produced a HR increase of ~50 beats/min.

As a supplemental protocol, we performed the transfer function analysis using binary white noise signals of 0–1 Hz ($Bin_{0\text{-}1}$), 0–3 Hz ($Bin_{0\text{-}3}$), and 0–5 Hz ($Bin_{0\text{-}5}$) in a random order (n = 5). At least a 15-min interval was allowed between the 20-min dynamic sympathetic stimulation trials. The amplitude of sympathetic stimulation was set so that 1-Hz tonic sympathetic stimulation produced a HR increase of ~50 beats/min.

Medetomidine has higher affinity to α_2-adrenergic receptors over α_1-adrenergic receptors compared with clonidine (α_2/α_1 = 1,620:1 for medetomidine, 220:1 for clonidine) (28). However, a preliminary experiment indicated that medetomidine was not as effective as

clonidine to modulate the transfer function from dynamic sympathetic stimulation to HR. Accordingly, we examined the effects of clonidine or medetomidine on myocardial interstitial NE release in response to 5-Hz tonic stimulation (2.5 V, 2-ms pulse width) of the right cardiac sympathetic nerve in vagotomized rabbits. Two microdialysis probes were implanted in the myocardium of the left ventricular free wall. Ringer solution was perfused at 2 μl/min. After a 2-h equilibrium period, we collected 5-min dialysate samples to measure the dialysate NE concentration as an index of myocardial interstitial NE levels (14, 15). High-performance liquid chromatography with electrochemical detection was used to quantify the NE concentration. After the sympathetic stimulation was performed under the control condition, clonidine or medetomidine was intravenously administered (1.5 $mg \cdot kg^{-1} \cdot h^{-1}$). Fifteen minutes later, the sympathetic stimulation was performed under the drug administration condition. Then the drug administration was ceased. Forty-five minutes later, the sympathetic stimulation was performed under the recovery condition. We used different rabbits for clonidine and medatomidine trials. We pooled six dialysate data for statistical analysis.

Data Analysis

Data were digitized at 200 Hz utilizing a 12-bit analog-to-digital converter and stored on the hard disk of a dedicated laboratory computer system. Mean values for HR and AP during dynamic sympathetic nerve stimulation were calculated by averaging the respective data over the stimulation period.

The transfer function from dynamic sympathetic nerve stimulation to HR response was estimated by the following procedures. Twenty minutes of input data (stimulation command) and output data (HR) were resampled at 8 Hz. The resampled data were segmented into eight 50% overlapping bins consisting of 2,048 data points each. The segment length was 256 s. For each segment, the linear trend was subtracted, and a Hanning window was applied. Fast-Fourier transform was then performed to obtain the frequency spectrum of nerve stimulation rate [$N(f)$] and that of HR [$HR(f)$] (5). The power spectral density of the nerve stimulation rate [$S_{N \cdot N}(f)$], that of HR [$S_{HR \cdot HR}(f)$], as well as the cross-spectral density between these two signals [$S_{N \cdot HR}(f)$], were averaged over the eight segments. Finally, the transfer function [$H(f)$] from sympathetic nerve stimulation rate to HR response was calculated using the following equation (2, 21).

$$H(f) = \frac{S_{N \cdot HR}(f)}{S_{N \cdot N}(f)} \quad (1)$$

Transfer function parameters were determined by fitting a second-order, low-pass filter to the estimated transfer function, according to previous studies (12, 13, 23). The second-order, low-pass filter with a pure dead time [$G(f)$] is expressed as

$$G(f) = \frac{K}{1 + 2\zeta \frac{f}{f_N} j + \left(\frac{f}{f_N} j\right)^2} \exp(-2\pi f j L) \quad (2)$$

where K is a steady-state gain, f_N is natural frequency (in Hz), ζ is a damping ratio, L is pure dead time (in s), and j indicates an imaginary unit. A schematic explanation for these transfer function parameters is provided in the APPENDIX. To estimate the parameters, an iterative nonlinear least squares fitting was performed to minimize the following error function.

$$\text{error} = \frac{\sum_{k=1}^{n} |G(f) - H(f)|^2}{\sum_{i=1}^{n} |H(f)|^2}, \quad f = f_0 \times k \quad (3)$$

where f_0 is the fundamental frequency of the discrete Fourier transform, $f_0 = 1/256 = 0.004$ Hz, and k is a frequency index. The n represents the upper limit of the frequency index determined from the range of sufficient input power in the sympathetic nerve stimulation; $n = 40$, $f_0 \times n = 0.156$ Hz.

To quantify the linear dependence of the HR response on the sympathetic nerve stimulation, the magnitude-squared coherence function [$\gamma^2(f)$] was calculated by the following equation (2, 21).

$$\gamma^2(f) = \frac{|S_{N \cdot HR}(f)|^2}{S_{N \cdot N}(f) \cdot S_{HR \cdot HR}(f)} \quad (4)$$

The coherence value ranges from zero to unity. The unity coherence value indicates a perfect linear dependence between the input and output signals, whereas zero coherence indicates a total independence between the two signals.

To facilitate the intuitive understanding of the HR response to dynamic sympathetic nerve stimulation, we calculated the step response from the estimated transfer function. The step response was obtained from the time integral of the system impulse response derived from the inverse Fourier transform of the transfer function. The steady-state response was calculated by averaging the step response during the last 10 s of the 128-s response. To characterize the rising speed of the step response, the initial slope for the response was calculated as follows. An analysis of linear regression with a slope and an intercept was performed on the initial data points of the step response while varying the number of data points from 2 to 1,024. The maximum slope obtained was used as the initial slope of the response. The linear regression was performed, including the portion of the dead time. Although including the dead time reduced the maximum slope, the effect was small because the number of data points that yielded the maximum slope (~90 points) was much larger than that for the dead time (<10 points). The step response of RRI was also calculated from the corresponding transfer function from sympathetic nerve stimulation to RRI.

Statistics

All data are presented as means ± SE. In *protocol 1*, mean HR, AP, and transfer function parameters were compared before and during yohimbine administration by paired *t*-tests. In *protocol 2*, the data were compared among control, lower dose, and higher dose clonidine conditions using a repeated-measures ANOVA followed by Dunnett's test against the single control (8). In the supplemental protocol of the transfer function analysis, the data were compared among $Bin_{0\text{-}1}$, $Bin_{0\text{-}3}$, and $Bin_{0\text{-}5}$ stimulus conditions using a repeated-measures ANOVA followed by Tukey test for all pairwise comparisons. In the supplemental protocol of the NE measurement, baseline NE levels were compared before and during drug administration using a paired *t*-test. The NE levels during sympathetic stimulation were compared among control, drug administration, and recovery conditions using a repeated-measures ANOVA followed by Dunnett's test against the control condition. In all of the statistical procedures, the difference was considered significant at $P < 0.05$.

RESULTS

Figure 2*A* represents a typical recording obtained from *protocol 1*. We stimulated the cardiac sympathetic nerve according to a binary white noise signal and recorded HR response under control condition and during yohimbine administration. The presynaptic α_2-adrenergic negative feedback mechanism functioned under the control condition but not during yohimbine administration. HR changed dynamically in response to the random sympathetic nerve stimulation under both conditions. Yohimbine increased the magnitude of HR variation. The augmentation of sympathetic effect was also observed in the RRI response. Although yohimbine decreased the mean level of HR in this animal, changes in mean HR

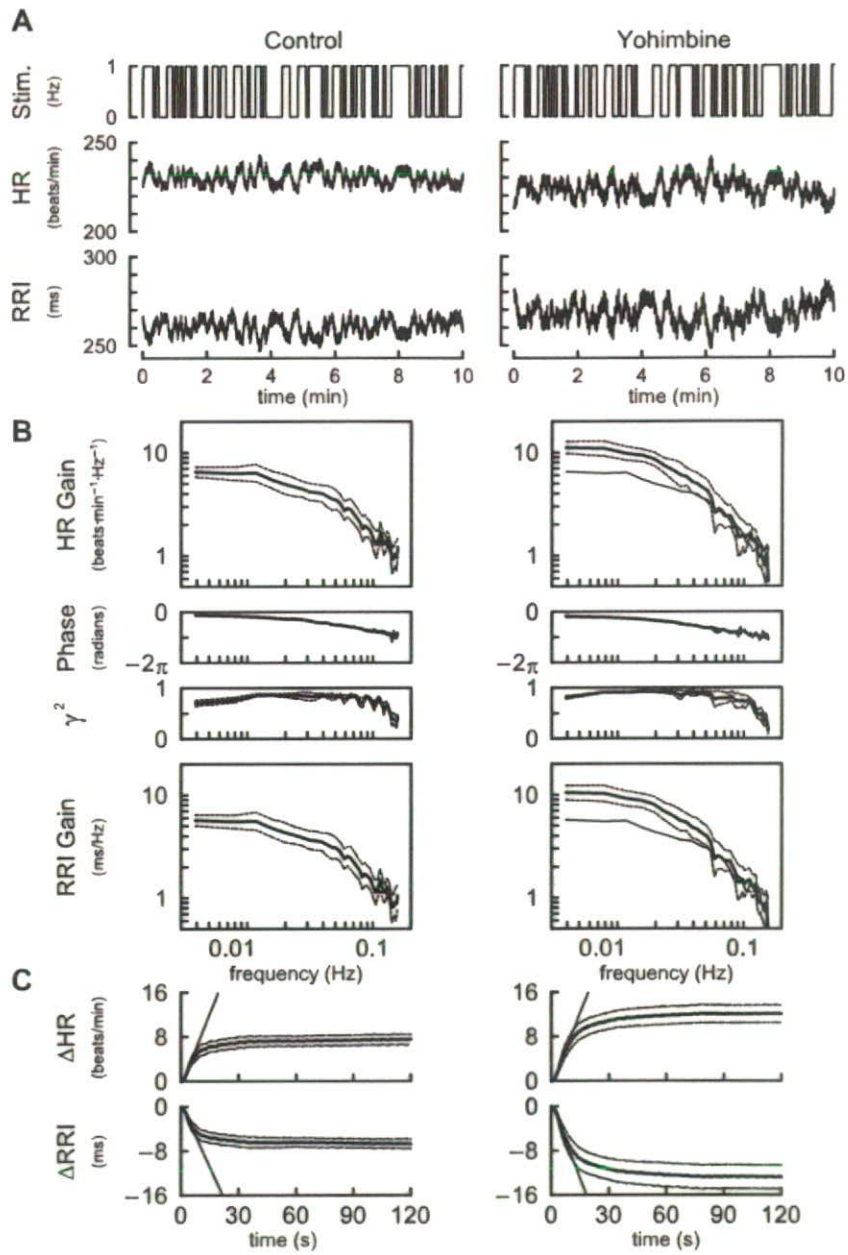

Fig. 2. *A:* representative recordings of cardiac sympathetic nerve stimulation rate (Stim; *top*), HR response (*middle*), and R-R interval (RRI) response (*bottom*) under conditions of control (*left*) and yohimbine administration (*right*) obtained in *protocol 1*. Yohimbine blocks the presynaptic α_2-adrenergic autoinhibition. The amplitude of HR variation and that of RRI variation become greater in the presence of yohimbine. *B:* transfer functions averaged over all animals in *protocol 1*. HR gain plots (*top*), phase plots (*second*), coherence functions (γ_2, *third*), and RRI gain plots (*bottom*). Yohimbine increases the dynamic gain in the frequency range between 0.004 and 0.04 Hz but not in the higher frequency range. The fine solid curve in the gain (*right*) duplicates the mean gain plot (*left*). *C:* step responses of HR (*top*) and RRI (*bottom*) calculated from the corresponding transfer functions. Yohimbine augments the steady-state response without affecting the initial slope of the response (fine oblique line). Bold, solid lines represent the mean, whereas dotted lines indicate means ± SE.

varied among the animals and were not significantly different between the control and yohimbine conditions.

Table 1 summarizes the mean HR and AP averaged from the six animals. The α_2-adrenergic blockade by yohimbine did not significantly affect the HR or AP before sympathetic nerve stimulation. Yohimbine also did not affect HR or AP significantly during the stimulation period.

Figure 2*B* illustrates the transfer functions averaged from the six animals in *protocol 1*. In the HR gain plots, the gain value was relatively constant <0.01 Hz and decreased >0.01 Hz, indicating low-pass filter characteristics of the HR response to sympathetic nerve stimulation. Yohimbine increased the HR gain from 7.1 ± 0.7 to 12.0 ± 1.7 beats·min^{-1}·Hz^{-1} at the lowest frequency of 0.004 Hz ($P < 0.05$). In contrast, yohimbine did not affect the HR gain value at 0.1 Hz (1.8 ± 0.4 vs. 1.7 ± 0.6 beats·min^{-1}·Hz^{-1}). The solid fine curve in the *right* panel duplicates the mean gain plot in the *left* panel as a reference. In the phase plots, the phase value approached zero radians at the lowest frequency and lagged with increasing frequency under both conditions. In the coherence function plots, the coherence was >0.8 in the frequency range from 0.01 to 0.08 Hz, suggesting that the HR response to sympathetic nerve stimulation in this frequency range can be explained reasonably well by linear dynamics for both conditions. Changes in the RRI gain plots were similar to those in the HR gain plots. Yohimbine increased the RRI gain from

Table 1. *Mean heart rate and arterial pressure before and during random stimulation of the cardiac sympathetic nerve*

	Control	Yohimbine
Heart rate, beats/min		
Before	259±15	244±13
During	264±15	254±17
Mean arterial pressure, mmHg		
Before	90±8	87±6
During	91±9	88±8

Values are means ± SE. Data were obtained after vagal and cardiac sympathetic nerves were cut. No statistically significant difference was detected between control vs. yohimbine values by paired *t*-tests.

6.0 ± 0.7 to 11.3 ± 1.9 ms/Hz at the lowest frequency of 0.004 ($P < 0.05$) but not at 0.1 Hz (1.8 ± 0.4 vs. 1.9 ± 0.8 ms/Hz). Given the inverse relationship between RRI and HR, the RRI phase plots (not shown) quite resembled to the corresponding HR phase plots except for the rotation by π radians.

Figure 2*C* represents the step responses of HR to sympathetic nerve stimulation calculated from the transfer functions shown in Fig. 2*B*. Yohimbine increased the steady-state response significantly (Table 2). The initial slope of the response, depicted by an oblique straight line, was not affected by yohimbine (Table 2). In the RRI step response, yohimbine augmented the steady-state response from −6.7 ± 0.9 to −12.6 ± 2.1 ms ($P < 0.05$) without affecting the initial slope (−0.71 ± 0.18 vs. −0.90 ± 0.23 ms/s).

Parameters of the transfer functions and step responses estimated in *protocol 1* are summarized in Table 2. The steady-state gain was significantly greater and the natural frequency was significantly lower in yohimbine condition compared with control. The damping coefficient and pure dead time did not differ significantly between the control and yohimbine conditions. Whereas the steady-state response was significantly increased by yohimbine, the initial slope of the step response was not significantly changed.

Figure 3*A* represents a typical recording of the sympathetic nerve stimulation and HR response obtained from *protocol 2*. The effects of α_2-adrenergic stimulation by clonidine were tested at two doses. Lower dose clonidine did not affect the magnitude of HR variation. Although lower dose clonidine decreased the mean HR in this animal, changes in the mean HR were not significantly different among the animals (Table 3). Higher dose clonidine significantly attenuated the magnitude of HR variation and also decreased mean HR. The attenuation of sympathetic effect was also observed in the RRI response during the high-dose clonidine administration.

Table 3 summarizes the mean HR and AP obtained from *protocol 2*. Higher dose, but not lower dose, clonidine significantly decreased the mean HR, both before and during cardiac sympathetic nerve stimulation. Clonidine did not affect mean AP significantly, before or during cardiac sympathetic nerve stimulation.

Figure 3*B* illustrates the transfer functions averaged from the five animals in *protocol 2*. Lower dose clonidine did not affect the transfer function significantly. In the HR gain plots, higher dose clonidine decreased the gain from 6.6 ± 0.9 to 2.7 ± 0.5 beats·min^{-1}·Hz^{-1} at the lowest frequency of 0.004 Hz ($P < 0.05$) and from 1.1 ± 0.2 to 0.5 ± 0.2 beats·min^{-1}·Hz^{-1} at the frequency of 0.1 Hz ($P < 0.05$). Higher dose clonidine did not affect the phase plot significantly. In the coherence function plots, the coherence was >0.8 in control and lower dose clonidine conditions and >0.7 in higher dose clonidine condition for the frequency range from 0.01 to 0.08 Hz, suggesting that the HR response to sympathetic nerve stimulation can be explained reasonably well by linear dynamics in all three conditions. Although relative change became smaller compared to the HR gain plots, the attenuation of transfer gain was also observed in the RRI gain plots. Higher-dose clonidine decreased the gain from 4.5 ± 0.7 to 2.8 ± 0.5 ms/Hz at the lowest frequency of 0.004 Hz ($P < 0.05$) and from 0.88 ± 0.19 to 0.04 ± 0.09 ms/Hz at the frequency of 0.1 Hz ($P < 0.05$).

Figure 3*C* represents the step responses of HR to sympathetic nerve stimulation calculated from the transfer functions shown in Fig. 3*B*. Lower dose clonidine did not affect either the steady-state response or the initial slope of the step response. In contrast, higher dose clonidine attenuated the steady-state response and also reduced the initial slope of the response. In the RRI step response, higher-dose clonidine attenuated the steady-state response from −4.9 ± 0.7 to −3.0 ± 0.6 ms ($P < 0.05$) with a significant reduction in the initial slope from −0.40 ± 0.07 to −0.23 ± 0.05 ms/s ($P < 0.05$).

Parameters of the transfer functions and step responses estimated in *protocol 2* are summarized in Table 4. The steady-state gain of the transfer function and the steady-state response of the corresponding step response were decreased by higher dose but not by lower dose clonidine. The initial slope of the step response was decreased by higher dose clonidine. The ratio of the steady-state response to the initial slope was unchanged. The natural frequency and the damping ratio of the transfer function were not affected by clonidine. The pure dead time of the transfer function was increased by lower dose, but not by higher dose, clonidine.

Figure 4*A* represents a typical recording of the sympathetic nerve stimulation and HR response obtained from the supplemental protocol. The binary white noise signals of the same sequence but different stimulus rate were applied. Increasing the stimulus rate augmented the magnitude of HR variation and increased mean HR. The increase was not proportional to the increase in the stimulus rate, however, because of the saturation of HR response to sympathetic nerve stimulation. The increase of RRI variation was not proportional to the increase in the stimulus rate either, suggesting that the saturation effect observed in the HR response was not an artifact of reciprocal relationship between RRI and HR.

Table 2. *Parameters of the transfer functions and step responses*

	Control	Yohimbine
K, beats·min^{-1}·Hz^{-1}	7.3±1.1	12.0±2.1*
f_N, Hz	0.081±0.012	0.055±0.008*
ζ	1.64±0.47	1.55±0.21
L, s	0.82±0.22	1.03±0.19
Fitting error, %	5.6±1.5	3.6±1.1
S, beats/min	7.2±0.8	12.2±1.7*
α, beats·min^{-1}·s^{-1}	0.93±0.23	0.94±0.22
S/α, s	9.1±1.4	14.4±1.9*

Values are means ± SE. K, steady-state gain; f_N, natural frequency; ζ, damping coefficient; L, pure dead time; S, steady-state response; α, initial slope; S/α, ratio of S to α. *$P < 0.05$ vs. control values.

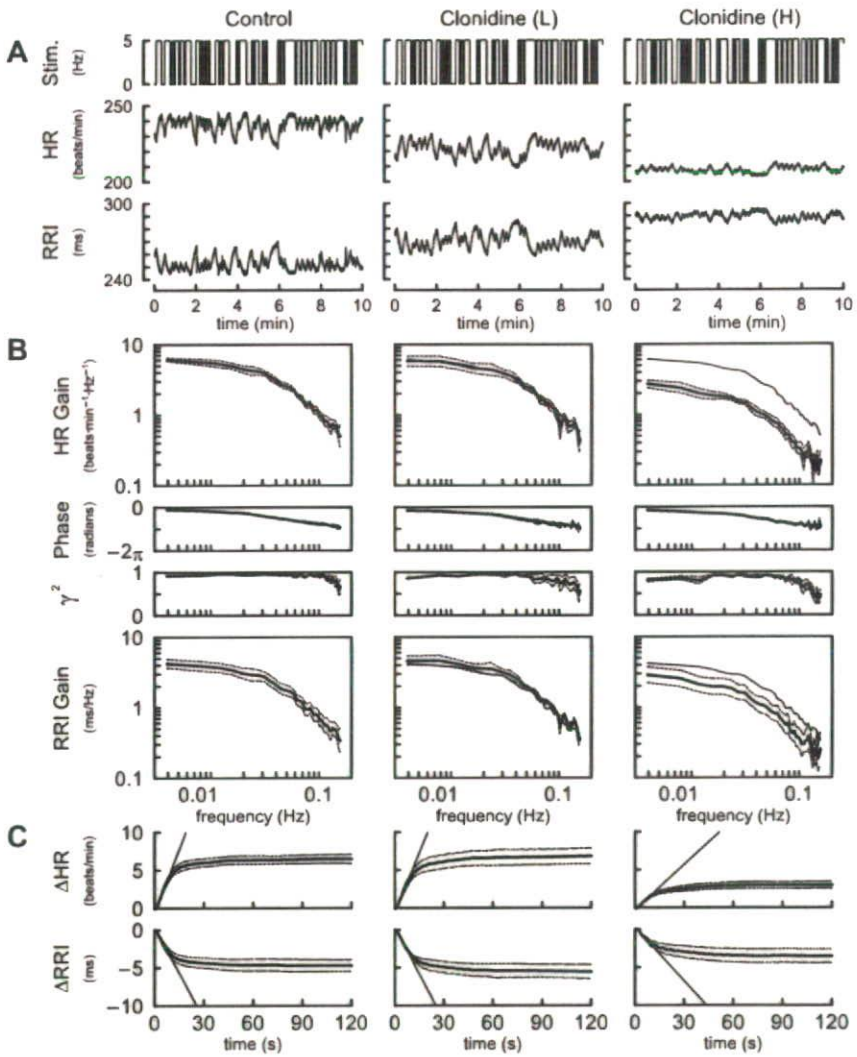

Fig. 3. *A:* representative recordings of cardiac sympathetic nerve stimulation rate (*top*), HR response (*middle*), and RRI response (*bottom*) under conditions of control (*left*), lower-dose clonidine (0.3 $mg \cdot kg^{-1} \cdot h^{-1}$; *middle*), and higher-dose clonidine (1.5 $mg \cdot kg^{-1} \cdot h^{-1}$; *right*) obtained in *protocol 2*. Clonidine activates the presynaptic α_2-adrenergic inhibition independent of the amount of norepinephrine released at the sympathetic nerve terminals. The amplitude of HR variation becomes smaller, and the mean level of HR becomes lower in the presence of higher-dose clonidine. The amplitude of RRI response also became smaller under higher-dose clonidine condition. *B:* transfer functions averaged over all animals in *protocol 2*. HR gain plots (*top*), phase plots (*second*), coherence functions (γ_2, *third*), and RRI gain plots (*bottom*). Lower-dose clonidine does not affect the transfer function significantly. Higher-dose clonidine decreases the dynamic gain in the whole frequency range (0.004 to 0.2 Hz). The fine solid curves in the gain plots (*middle* and *right*) duplicate the mean gain plot (*left*). *C:* step responses of HR (*top*) and RRI (*bottom*) calculated from the corresponding transfer functions. Lower-dose clonidine does not affect the step response significantly. Higher-dose clonidine attenuates the steady-state response accompanied by a decrease in the initial slope of the response (fine oblique line). Bold, solid lines represent the mean, whereas dotted lines indicate means ± SE.

Table 5 summarizes the mean HR and AP obtained from the supplemental protocol. There were no significant differences in mean HR and AP before cardiac sympathetic nerve stimulation. Mean HR was higher in $Bin_{0\text{-}3}$ and $Bin_{0\text{-}5}$ than in $Bin_{0\text{-}1}$ condition. Mean AP did not differ among the three conditions.

Figure 4*B* illustrates the transfer function averaged from the five animals in the supplemental protocol. The contour of HR gain plots showed an approximately downward shift with increase in the stimulus rate of the binary white noise signal, indicating that the augmentation of the HR variation seen in Fig. 4*A* was not proportional to the increase in the stimulus rate. No significant differences were noted in the phase plot. The coherence values were slightly decreased in all frequencies with increase in the stimulus rate of the binary white noise signal, suggesting that the HR response became saturated and the linearity between the stimulation and the HR response was

Table 3. *Mean heart rate and arterial pressure before and during random stimulation of the cardiac sympathetic nerve*

	Control	Clonidine (L)	Clonidine (H)
Heart rate, beats/min			
Before	277±16	250±15	232±20*
During	299±14	271±14	246±27*
Mean arterial pressure, mmHg			
Before	95±6	77±8	113±9
During	96±6	79±9	115±13

Values are means ± SE. Data were obtained after vagal and cardiac sympathetic nerves were cut. *$P < 0.05$ vs. control values by Dunnett's test.

Table 4. *Transfer function parameters and step responses*

	Control	Clonidine (L)	Clonidine (H)
K, $beats \cdot min^{-1} \cdot Hz^{-1}$	6.4±0.8	6.8±1.1	2.7±0.5*
f_N, Hz	0.066±0.017	0.070±0.016	0.059±0.013
ζ	1.56±0.37	1.72±0.23	1.55±0.20
L, s	0.56±0.17	1.24±0.20*	1.03±0.18
Fitting error, %	2.9±1.2	4.2±1.5	5.5±2.3
S, beats/min	6.3±0.8	6.8±1.0	2.8±0.5*
α, $beats \cdot min^{-1} \cdot s^{-1}$	0.56±0.07	0.51±0.04	0.22±0.06*
S/α, s	11.2±0.7	13.1±1.3	13.8±1.2

Values are means ± SE. *$P < 0.05$ vs. control values.

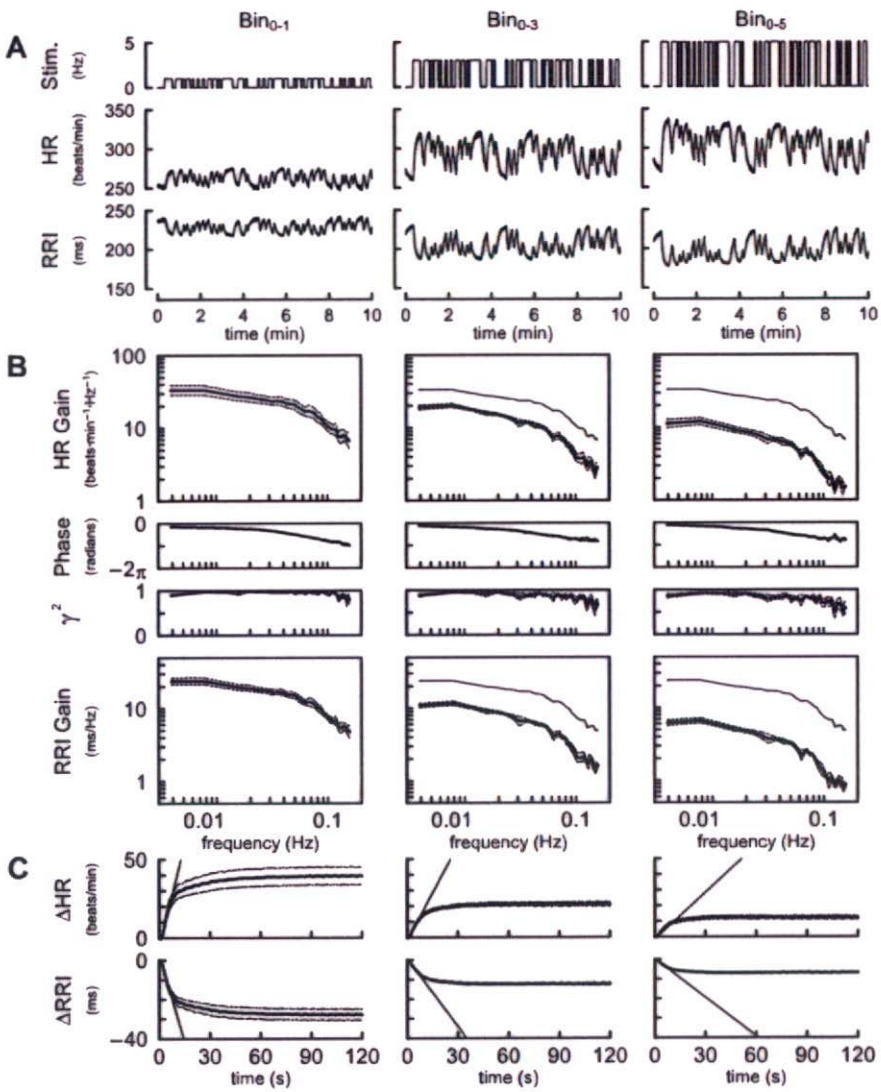

Fig. 4. *A*: representative recordings of cardiac sympathetic nerve stimulation rate (*top*), HR response (*middle*), and RRI response (*bottom*) obtained by differing the stimulus rate of the binary white noise signal. Bin_{0-1}, binary white noise between 0 and 1 Hz; Bin_{0-3}, binary white noise between 0 and 3 Hz; Bin_{0-5}, binary white noise between 0 and 5 Hz. Increasing the stimulus rate of the binary white noise signal augments the magnitude of HR response and increased mean HR. The RRI response was also increased with increasing the stimulus rate. *B:* transfer functions averaged over all animals in the supplemental protocol. HR gain plots (*top*), phase plots (*second*), coherence functions (γ_2, *third*), and RRI gain plots (*bottom*). Increasing the stimulus rate of the binary white noise signal decreases the dynamic gain in the whole frequency range (0.004 to 0.2 Hz). The fine solid curves in the gain plots (*middle* and *right*) duplicate the mean gain plot (*left*). *C:* step responses of HR (*top*) and RRI (*bottom*) calculated from the transfer functions. Increasing the stimulus rate of the binary white noise signal attenuates the steady-state response accompanied by a decrease in the initial slope of the response (fine oblique line). Bold, solid lines represent the mean, whereas dotted lines indicate means ± SE.

slightly reduced in Bin_{0-3} and Bin_{0-5} compared with that in Bin_{0-1} condition. The contour of RRI gain plots also showed approximately downward shift with increasing the stimulus rate of the binary white noise signal.

Figure 4*C* represents the step response of HR to sympathetic nerve stimulation calculated from the transfer functions shown in Fig. 4*B*. The increase in the stimulus rate of the binary white noise signal attenuated the steady-state response and also reduced the initial slope of the response. In the RRI step

Table 5. *Mean heart rate and arterial pressure before and during random stimulation of the cardiac sympathetic nerve*

	Bin_{0-1}	Bin_{0-3}	Bin_{0-5}
Heart rate, beats/min			
Before	268±6	269±7	266±5
During	292±8	330±9*	341±11*
Mean arterial pressure, mmHg			
Before	84±7	82±5	88±12
During	94±7	94±7	95±9

Values are means ± SE. Data were obtained after vagal and cardiac sympathetic nerves were cut. Bin_{0-1}, Bin_{0-3}, and Bin_{0-5}: binary white noise signals of 0–1, 0–3, and 0–5 Hz, respectively. *$P < 0.01$ vs. Bin_{0-1} values by Tukey test. There were no significant differences in parameters between Bin_{0-3} and Bin_{0-5}.

Table 6. *Transfer function parameters and step responses*

	Bin_{0-1}	Bin_{0-3}	Bin_{0-5}
K, beats·min^{-1}·Hz^{-1}	36.2±4.9	20.0±1.1†	11.8±1.1†
f_N, Hz	0.098±0.009	0.079±0.006*	0.078±0.006*
Z	1.56±0.04	1.68±0.04*	1.68±0.05*
L, s	0.95±0.01	0.97±0.01	0.97±0.01
Fitting error, %	4.8±1.1	3.2±0.8	3.5±0.5
S, beats/min	40.9±5.1	22.1±1.6†	12.8±1.4†
α, beats·min^{-1}·s^{-1}	4.23±0.61	2.00±0.21†	1.20±0.17†
S/α, s	9.9±0.5	11.3±0.8	10.8±0.8

Values are means ± SE. †$P < 0.01$ and *$P < 0.05$ vs. Bin_{0-1} values by Tukey test. There were no significant differences in parameters between Bin_{0-3} and Bin_{0-5}.

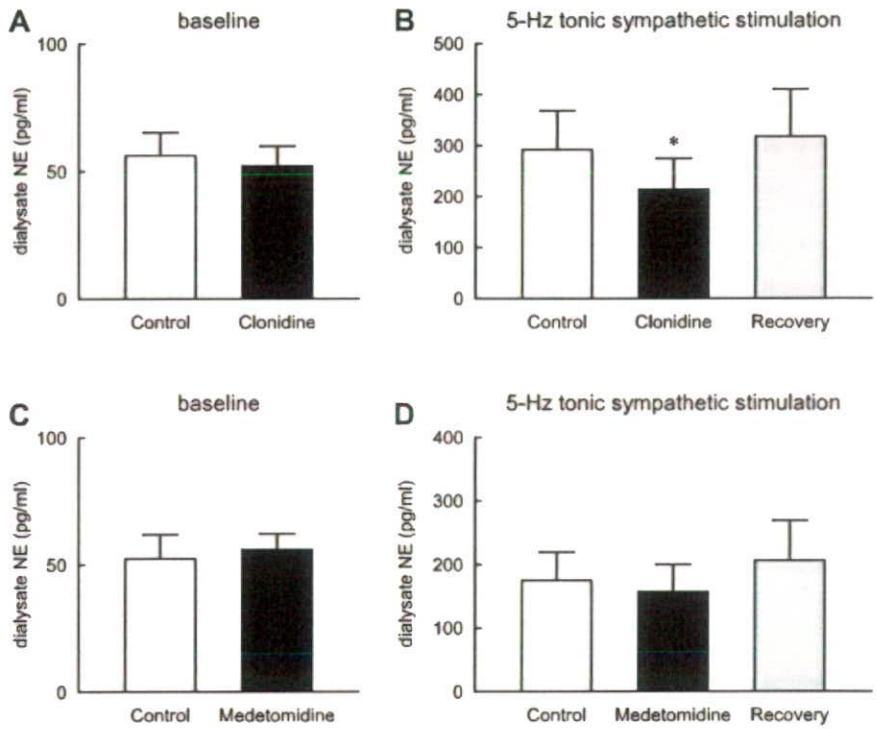

Fig. 5. Effects of clonidine (1.5 mg·kg^{-1}·h^{-1} iv) or medetomidine (1.5 mg·kg^{-1}·h^{-1} iv) on the myocardial interstitial norepinephrine (NE) release in response to 5-Hz tonic cardiac sympathetic nerve stimulation. Data were obtained after sectioning vagal and cardiac sympathetic nerves. Clonidine administration does not affect baseline levels of NE (*A*), but significantly attenuates the stimulation-induced NE release (*B*). *C*: medetomidine administration does not affect baseline levels of NE. *D*: it does not attenuate the stimulation-induced NE release significantly. Values are means ± SE. *$P < 0.05$ from control.

response, the steady-state response was attenuated from -27.6 ± 2.8 to -12.2 ± 0.7 ($P < 0.01$) and -6.7 ± 0.4 ($P < 0.01$) ms during Bin_{0-3} and Bin_{0-5}, respectively. The initial slope was attenuated from -3.0 ± 0.3 to -1.1 ± 0.1 ($P < 0.01$) and -0.65 ± 0.06 ($P < 0.01$) ms/s during Bin_{0-3} and Bin_{0-5}, respectively.

Parameters of the transfer functions and step responses estimated in the supplemental protocol are summarized in Table 6. The steady-state gain of the transfer function and the steady-state response of the corresponding step response decreased with increase in the stimulus rate of the binary white noise sequence. Although the initial slope of the step response significantly decreased with increase in the stimulus rate of the binary white noise signal, the ratio of the steady-state response to the initial slope was unchanged. The natural frequency was lower and the damping coefficient was greater in Bin_{0-3} and Bin_{0-5} than Bin_{0-1} condition. The pure dead time of the transfer function did not differ among the three conditions.

Figure 5 summarizes the results of the supplemental protocol of NE measurement. Baseline levels of myocardial interstitial NE did not differ before and during clonidine administration (Fig. 5*A*). Clonidine administration attenuated the sympathetic stimulation-induced NE release to 75.8 ± 5.4% of the control ($P < 0.05$) (Fig. 5*B*). Baseline NE levels did not differ before and during medetomidine administration (Fig. 5*C*). Medetomidine did not attenuate the sympathetic stimulation-induced NE release significantly (92.0 ± 6.7% of the control, not significant) (Fig. 5*D*).

Simulation Study

To explore possible mechanisms for the observed differences between the presynaptic α_2-adrenergic autoinhibition and the pharmacologic augmentation of the presynaptic inhibition via the α_2-adrenergic receptors, we performed a simulation on the negative feedback regulation of the HR response to the sympathetic nerve stimulation. With reference to Fig. 6*A*, H_{FW} and H_{FB} represent the transfer functions of the forward path and the feedback path, respectively. A step input signal represents the sympathetic nerve stimulation. Both signals from presynaptic α_2-adrenergic autoinhibition and pharmacologic augmentation of the presynaptic inhibition attenuate the input signal via the same α_2-adrenergic receptors. Because the amount of neurotransmitter release cannot become negative, a threshold operator (Th) is added. The threshold operator is described mathematically as follows.

$$\mathrm{Th}(x) = x \text{ when } x > 0, \text{ otherwise } \mathrm{Th}(x) = 0$$

The output from the threshold operator or the amount of neurotransmitter is then fed into H_{FW} to yield the output or change in HR and is also fed into H_{FB} to yield the feedback signal of presynaptic α_2-adrenergic autoinhibition. Since we administered clonidine ~15 min before sympathetic nerve stimulation, the effect of clonidine should have reached the steady state at the time of sympathetic nerve stimulation. Accordingly, we treated the pharmacologic augmentation of the presynaptic inhibition as a constant input. The magnitude of pharmacologic augmentation of the presynaptic inhibition was set arbitrarily to 0.5 to mimic the results of higher dose clonidine in *protocol 2*. The simulation was conducted using Matlab Simulink (The Mathworks, Natick, MA).

Yohimbine administration corresponds to severing the feedback path, i.e., setting $H_{FB} = 0$ in the simulation. Under this condition, the transfer function from the input to output becomes H_{FW}. Therefore, we modeled H_{FW} using the second-order, low-pass filter with pure dead time (*Eq. 3*) with the

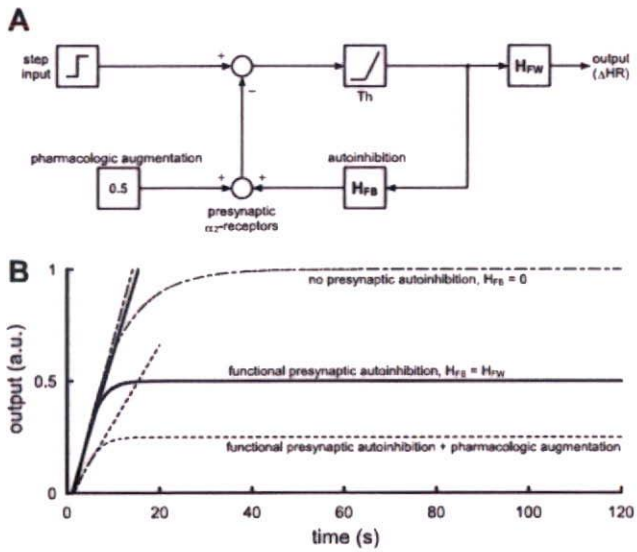

Fig. 6. Possible theoretical explanation for the differential effects of presynaptic α_2-adrenergic autoinhibition and pharmacologic augmentation of presynaptic α_2-adrenergic inhibition on the HR response to sympathetic nerve stimulation. *A:* a simulation model for the HR step response to a step input in the sympathetic nerve activity. H_{FW}, transfer function of the forward path; H_{FB}, transfer function of the feedback path; Th, a threshold operator (see main text for details). *B:* simulation results under conditions of no presynaptic inhibition (dash-dot line; H_{FB} = 0 and pharmacologic augmentation of presynaptic inhibition = 0, corresponding to the yohimbine administration condition), functional presynaptic α_2-adrenergic autoinhibition (solid line; H_{FB} = H_{FW} and pharmacologic augmentation of presynaptic inhibition = 0, corresponding to the control condition), and functional presynaptic α_2-adrenergic autoinhibition plus pharmacologic augmentation of the presynaptic inhibition (dotted line; H_{FB} = H_{FW} and pharmacologic augmentation of presynaptic inhibition = 0.5, corresponding to the higher-dose clonidine condition). The presynaptic α_2-adrenergic autoinhibition does not attenuate the initial slope of the step response. In contrast, the pharmacologic augmentation of the presynaptic inhibition attenuates the initial slope of the step response.

settings of f_N = 0.055, ζ = 1.55, and L = 0.94 (Table 2, yohinbine). The gain was set at unity for simplicity. With this setting, we calculated the output response to the unit step input without the presynaptic inhibition (Fig. 6*B*, dash-dot line, corresponding to the yohimbine condition). The initial slope of the response, calculated from the linear regression analysis described in the method section, was 0.0763 arbitrary units (AU)/s. Next, we set H_{FB} = H_{FW} and performed a simulation of the condition with the presynaptic α_2-adrenergic autoinhibition (Fig. 6*B*, solid line, corresponding to the control condition). The presynaptic α_2-adrenergic autoinhibition attenuates the steady-state response without significantly affecting the initial slope of the response (0.0695 AU/s). Finally, we set the pharmacologic augmentation of the presynaptic inhibition to 0.5 on top of the functioning H_{FB}. The simulation result (Fig. 6*B*, dotted line, corresponding to the higher dose clonidine condition) demonstrates that pharmacologic augmentation of the presynaptic inhibition attenuates the steady-state response accompanied by a reduction in the initial slope of the response (0.0346 AU/s).

DISCUSSION

We compared the blockade and activation of the presynaptic α_2-adrenergic receptors and found a difference between the presynaptic α_2-adrenergic autoinhibition and the pharmacologic augmentation of the presynaptic inhibition in terms of HR response to sympathetic nerve stimulation. The presynaptic α_2-adrenergic autoinhibition showed a limiter-like operation that restricts the steady-state response without affecting the initial slope of the response. In contrast, the pharmacologic augmentation of presynaptic inhibition showed an attenuator-like operation that reduces both the steady-state response and the initial slope of the response.

Comparison of Blocking and Activating the Presynaptic α_2-Adrenergic Receptors

Although the presynaptic α_2-adrenergic negative feedback has been known to attenuate the NE release and HR response to sympathetic nerve stimulation (9, 21, 26, 27, 29, 30, 31), the dynamic nature of the negative feedback remained to be elucidated. As shown in Fig. 2*C*, the blockade of α_2-adrenergic receptors by yohimbine increased the steady-state response without significantly affecting the initial slope of the HR step response (Table 2). That is to say, the presynaptic α_2-adrenergic autoinhibition of the presynaptic inhibition attenuates the steady-state response without sacrificing the rising speed of HR response to sympathetic nerve stimulation under control condition. These characteristics of the presynaptic α_2-adrenergic autoinhibition conform to the limiter-like operation shown in Fig. 1*A*. In contrast, pharmacologic augmentation of the presynaptic inhibition by higher dose clonidine reduced the steady-state response accompanied by a decrease in the initial slope of the HR step response (Fig. 3*C*). The ratio of the steady-state response to the initial slope was not changed significantly by higher dose clonidine (Table 4), suggesting that attenuation of the initial slope was proportional to that of the steady-state response. These characteristics of the pharmacologic augmentation of the presynaptic inhibition conform to the attenuator-like operation shown in Fig. 1*B*. Rapid effector response is one of the most important hallmarks of neural regulation compared with humoral regulation. The findings of the present study suggest that presynaptic α_2-adrenergic autoinhibition, but not pharmacologic augmentation of the presynaptic α_2-adrenergic inhibition, prevents excess NE outflow at the sympathetic nerve terminals without compromising the rapidity of effector response. The simulation results suggest that the initial slope of the response decreases when presynaptic inhibition occurs, independent of the negative feedback mechanism (Fig. 6*B*). On the other hand, the initial slope of the response does not decrease significantly when the presynaptic inhibition occurs through the negative feedback mechanism.

α_2-Adrenergic receptors are classified as α_{2A}-, α_{2B}-, and α_{2C}-subtypes based on gene encodings (26). Furthermore, the different ligand binding characteristics of the α_{2A}-subtype give rise to the pharmacological subtype of α_{2A} in humans, rabbits, and pigs and that of α_{2D} in rats, mice, and guinea pigs (26). The α_{2A} and α_{2D} may be considered as "orthologous" α_2-receptors, with only one being present in any given species (27). In the sympathetic nerve, α_{2A}- and α_{2C}-receptors operate as presynaptic inhibitory autoreceptors, whereas α_{2B}-receptors are located on postsynaptic cells to mediate the effects of catecholamine, such as vasoconstriction (26). In tissue slices from mouse atria, α_{2A}-receptors inhibit NE release from sympathetic nerves primarily at high-stimulation rates (1–2 Hz), whereas

α_{2C}-receptors can operate at very low stimulation rates (0.05–0.1 Hz) (10). Because α_2-receptors in the rabbit heart are characterized as α_{2A}, changes in the transfer function from sympathetic nerve stimulation to HR response observed in the present study are most likely mediated by α_{2A}-receptors.

Clonidine administration (5 μg/kg bolus followed by 30 $\mu g \cdot kg^{-1} \cdot h^{-1}$ iv) attenuated the sympathetic outflow from the central nervous system in rabbits (35). However, lower dose clonidine at 0.3 $mg \cdot kg^{-1} \cdot h^{-1}$ failed to significantly affect the steady-state response or the initial slope of the HR step response in the present study (Fig. 3*B*, Table 4), suggesting a difference in clonidine sensitivity between the central and peripheral sympathetic nervous systems. Another factor that should be taken into account is the operating range of the HR control (i.e., mean HR during dynamic sympathetic stimulation). As an example, tonic vagal stimulation decreased mean HR during dynamic sympathetic stimulation, which increased the dynamic gain of sympathetic HR control via nonlinear sigmoidal input-output nature between autonomic activities and HR (12, 13). Therefore, the decrease in the mean HR during lower dose clonidine, although it was statistically insignificant (Table 3), should have an effect of increasing the dynamic gain of the sympathetic HR control. Such an effect might have counterbalanced the effect of reducing the dynamic gain via presynaptic inhibition during the lower dose clonidine administration. Although higher dose clonidine decreased mean HR before and during sympathetic nerve stimulation, mean AP did not decrease compared with lower dose clonidine (Table 3). The discrepancy between the changes in mean HR and AP may be due to direct vasoconstriction by higher dose clonidine through α-adrenergic stimulation.

Transfer Function Analysis vs. Step Response Analysis

In a previous study, our laboratory performed a transfer function analysis on the sympathetic HR control using a binary white noise signal (12, 23). The transfer function is a frequency-domain representation of the system dynamic characteristics over a wide frequency range and is useful for understanding the behavior of the system in response to a variety of input signals (3, 7, 21). Notwithstanding the theoretical advantages of the transfer function, the frequency-domain representation may be somewhat unfamiliar to most physiologists. Therefore, we calculated the step responses corresponding to the transfer functions. As can be seen in Figs. 2, *B* and *C* and 3, *B* and *C*, changes in transfer function in the lower frequency range reflect the steady-state response in the step response. Changes in transfer function in the higher frequency reflect the initial transient response in the step response. Because the step response and the transfer function are mathematically interchangeable, both the transfer function and the step response provide comparable information on the system dynamic characteristics.

In a previous study, our laboratory has shown that increasing mean stimulus rate of the Gaussian white noise decreased the steady-state gain of the transfer function from sympathetic nerve stimulation to HR without affecting the natural frequency or damping coefficient significantly (23). Increasing the stimulus rate of the binary white noise signal also caused an approximately parallel downward shift in the gain plot (Fig. 4*B*). The transfer function parameters, however, showed a decrease in the natural frequency and an increase in the damping coefficient (Table 6). The higher natural frequency in $Bin_{0\text{-}1}$ than in $Bin_{0\text{-}5}$ condition may account for the higher natural frequency in *protocol 1* ($Bin_{0\text{-}1}$ was used for sympathetic stimulation) than in *protocol 2* ($Bin_{0\text{-}5}$ was used for sympathetic stimulation) observed under control conditions. Notwithstanding the differences in the natural frequency and the damping coefficient, the ratio of the step response to the initial slope was not changed significantly by the difference in the stimulus rate of the binary white noise signal. Therefore, yohimbine-induced changes in the ratio of the step response to the initial slope observed in *protocol 1* (Table 1) cannot be explained by changes in the magnitude of sympathetic effect on HR.

Limitations

The present study has several limitations. First, we performed the experiment under anesthetic conditions. However, because we compared the effects of yohimbine and clonidine on the sympathetic HR control under the same anesthetic

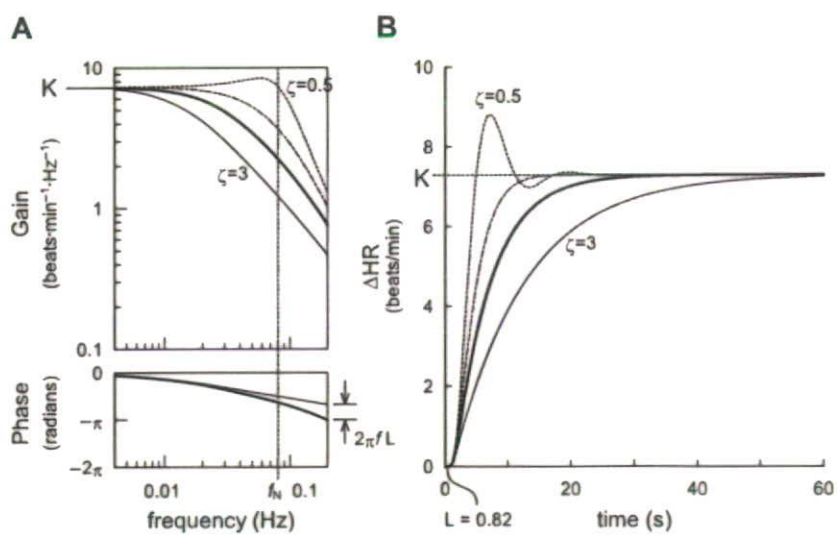

Fig. 7. Schematic explanation for the frequency response of a second-order, low-pass filter with pure dead time (*L*; *A*), and the corresponding step response (*B*). *K*, dynamic gain; f_N, natural frequency; ζ, damping ratio. See APPENDIX for details.

condition, the interpretation of the observed changes in the transfer function may be reasonable. Second, the simulation model in Fig. 6*A* is not the only model that can be applied to the observed results. Although the model is convenient to explain many aspects of the observed results, other models may also be applicable to the present observation. Third, clonidine can affect HR through non-α_2-adrenergic mechanisms. For instance, clonidine caused bradycardia in α_{2ABC}-knockout mouse via direct inhibition of cardiac hyperpolarization-activated cyclic nucleotide-gated pacemaker channels (16). While we tried to use medetomidine instead of clonidine, medetomidine did not attenuate myocardial interstitial NE release in response to sympathetic nerve stimulation significantly, at least, at the same dose as clonidine (Fig. 5). Further studies using other agonists might be required to confirm our observations. Finally, we used a weak stimulus rate (0 to 1 Hz) for the yohimbine protocol. Although we had examined the effect of yohimbine using a strong stimulus rate (0–5 Hz) in a preliminary study, the steady-state gain of the transfer function did not increase much (8.4 ± 1.7 vs. 9.0 ± 1.7 beats·min^{-1}·Hz^{-1}, n = 3). Under such strong stimulus condition, the saturation of HR response might have masked the effect of presynaptic inhibition. Therefore, the result of *protocol 1* should be carefully interpreted in view of the existence of a stimulus rate-drug interaction effect.

Conclusions

The presynaptic α_2-adrenergic autoinhibition attenuates the dynamic HR response to sympathetic nerve stimulation in the low-frequency range (0.004–0.04 Hz) but not in the high-frequency range (0.05–0.15 Hz). In the time domain, the presynaptic α_2-adrenergic autoinhibition attenuates the steady-state response without affecting the slope of the response in the HR step response (a limiter-like operation). In contrast, pharmacologic augmentation of presynaptic α_2-adrenergic inhibition attenuates the dynamic HR response to sympathetic nerve stimulation in a frequency-independent manner. In the time domain, pharmacologic augmentation of the presynaptic inhibition attenuates not only the steady-state response but also the initial slope of the HR step response (an attenuator-like operation). Presynaptic α_2-adrenergic autoinhibition would be favorable for limiting excess NE outflow at the sympathetic nerve terminals without compromising the rapidity of effector response.

APPENDIX

Mathematical Modeling of the Sympathetic HR Response

To describe the estimated transfer function, we used a second-order, low-pass filter with pure dead time (L). Figure 7*A* shows the frequency response of a second-order, low-pass filter with L. Figure 7*B* shows the corresponding step response. The step response is calculated for 1-Hz sympathetic nerve stimulation. The steady-state gain (K) of the transfer function represents the value of transfer gain as the frequency approaches zero. The K corresponds to the steady-state response in the step-response representation. The natural frequency (f_N) determines the upper frequency limit of the low-pass filter. For instance, if the f_N were 10 times higher, the frequency axis in Fig. 7*A* would have to be scaled by a factor of 10, indicating that the system could respond to 10-fold higher frequency input. The phase plot in Fig. 7*A* indicates that, at the f_N, the output is delayed by $\pi/2$ radians relative to the input, in the absence of the L. The maximum phase delay of the second-order, low-pass filter is π radians in the absence of L. The L is needed to account for the phase difference between the estimated transfer function and the second-order, low-pass filter. In Fig. 7*B*, the L corresponds to the time difference between the onset of the step input and the onset of the response. The damping coefficient (ζ) characterizes the system response around the f_N. As an example, the gain plot shows a slight peak around f_N when ζ = 0.5 (dotted line). Figure 7*B* shows that a ζ of 0.5 causes an initial overshoot in response to a step change in the input. A system with $\zeta <$ 1 is called underdamped. On the other hand, the gain plot shows more gradual decrease around f_N when ζ = 3 (fine solid line). Figure 7*B* shows that the system responds sluggishly when ζ = 3. A system with $\zeta > 1$ is called overdamped. A system with ζ = 1 is called critically damped (dash-dot line). The ζ of the estimated transfer functions ranged from 1.55 to 1.72 in the present study, indicating that the sympathetic HR control system is overdamped. The solid line represents the second-order, low-pass filter with ζ = 1.64 and L = 0.82 that is derived from the mean value obtained under control condition in *protocol 1*.

GRANTS

This study was supported by "Health and Labour Sciences Research Grant for Research on Advanced Medical Technology," "Health and Labour Sciences Research Grant for Research on Medical Devices for Analyzing, Supporting and Substituting the Function of Human Body," and "Health and Labour Sciences Research Grant H18-Iryo-Ippan-023" from the Ministry of Health, Labour and Welfare of Japan; "Program for Promotion of Fundamental Studies in Health Science" from the National Institute of Biomedical Innovation; and "Ground-based Research Announcement for Space Utilization" promoted by the Japan Space Forum.

REFERENCES

1. **Altman JD, Trendelenburg AU, MacMillan L, Bernstein D, Limbird L, Starke K, Kobilka BK, Hein L.** Abnormal regulation of the sympathetic nervous system in α_{2A}-adrenergic receptor knockout mice. *Mol Pharmacol* 56: 154–161, 1999.
2. **Bendat JS, Piersol AG.** Single-input/output relationships. In: *Random Data Analysis and Measurement Procedures* (3rd Ed.). New York: Wiley, 2000, p. 189–217.
3. **Berger RD, Saul JP, Cohen RJ.** Transfer function analysis of autonomic regulation. I. Canine atrial rate response. *Am J Physiol Heart Circ Physiol* 256: H142–H152, 1989.
5. **Brigham EO.** FFT transform applications. In: *The Fast Fourier Transform and Its Applications*. Englewood Cliffs, NJ: Prentice-Hall, 1988, p. 167–203.
6. **Buhler FR, Bolli P, Amann WF, Erne P, Kiowski W.** Sympathetic nervous system in essential hypertension and antihypertensive response to α_2-adrenoceptor stimulation. *J Cardiovasc Pharmacol* 6: S753–S756, 1984.
7. **Franklin GF, Powell JD, and Emani-Naeini A.** Dynamic models and dynamic response. In: *Feedback Control of Dynamic Systems* (2nd Ed.). Boston, MA: Addison-Wesley, 1991, p. 17–144.
8. **Glantz SA.** *Primer of Biostatistics* (5th Ed.). New York: McGraw-Hill, 2002.
9. **Grossman E, Chang PC, Hoffman A, Tamrat M, Goldstein DS.** Evidence for functional α_2-adrenoceptors on vascular sympathetic nerve endings in the human forearm. *Circ Res* 69: 887–897, 1991.
10. **Hein L, Altman JD, Kobilka BK.** Two functionally distinct α2-adrenergic receptors regulate sympathetic neurotransmission. *Nature* 402: 181–184, 1999.
11. **Jie K, van Brummelen P, Vermey P, Timmermans PB, van Zwieten PA.** Modulation of noradrenaline release by peripheral presynaptic α_2-adrenoceptors in humans. *J Cardiovasc Pharmacol* 9: 407–413, 1987.
12. **Kawada T, Ikeda Y, Sugimachi M, Shishido T, Kawaguchi O, Yamazaki T, Alexander J Jr, Sunagawa K.** Bidirectional augmentation of heart rate regulation by autonomic nervous system in rabbits. *Am J Physiol Heart Circ Physiol* 271: H288–H295, 1996.
13. **Kawada T, Sugimachi M, Shishido T, Miyano H, Sato T, Yoshimura R, Miyashita H, Nakahara T, Alexander J Jr, Sunagawa K.** Simultaneous identification of static and dynamic vagosympathetic interactions in regulating heart rate. *Am J Physiol Regul Integr Comp Physiol* 276: R782–R789, 1999.

14. **Kawada T, Yamazaki T, Akiyama T, Sato T, Shishido T, Sugimachi M, Inagaki M, Alexander J Jr, Sunagawa K.** Liquid chromatographic determination of myocardial interstitial epinephrine. *J Chromatogr B Biomed Sci Appl* 714: 375–378, 1998.
15. **Kawada T, Yamazaki T, Akiyama T, Sato T, Shishido T, Yoshimura R, Inagaki M, Tatewaki T, Sugimachi M, Sunagawa K.** Local epinephrine release in the rabbit myocardial interstitium in vivo. *J Auton Nerv Syst* 78: 94–98, 2000.
16. **Knaus A, Zong X, Beetz N, Jahns R, Lohse MJ, Biel M, Hein L.** Direct inhibition of cardiac hyperpolarization-activated cyclic nucleotide-gated pacemaker channels by clonidine. *Circulation* 115: 872–880, 2007.
17. **Langer SZ.** 25 years since the discovery of presynaptic receptors, present knowledge and future perspectives. *Trends Pharmacol Sci* 18: 95–99, 1997.
18. **Langer SZ.** Presence and physiological role of presynaptic inhibitory α_2-adrenoreceptors in guinea pig atria. *Nature* 294: 671–672, 1981.
19. **Langer SZ, Adler-Graschinsky E, Giorgi O.** Physiological significance of α-adrenoceptor-mediated negative feedback mechanism regulating noradrenaline release during nerve stimulation. *Nature* 265: 648–650, 1977.
20. **Langer SZ.** Presynaptic regulation of catecholamine release. *Biochem Pharmacol* 23: 1793–1800, 1974.
21. **Marmarelis PZ, Marmarelis VZ.** The white noise method in system identification. In: *Analysis of Physiological Systems*. New York: Plenum, 1978, p. 131–221.
22. **Miyamoto T, Kawada T, Yanagiya Y, Takaki H, Inagaki M, Sugimachi M, Sunagawa K.** Cardiac sympathetic nerve stimulation does not attenuate dynamic vagal control of heart rate via α-adrenergic mechanism. *Am J Physiol Heart Circ Physiol* 287: H860–H865, 2004.
23. **Nakahara T, Kawada T, Sugimachi M, Miyano H, Sato T, Shishido T, Yoshimura R, Miyashita H, Inagaki M, Alexander J Jr, Sunagawa K.** Neuronal uptake affects dynamic characteristics of heart rate response to sympathetic stimulation. *Am J Physiol Regul Integr Comp Physiol* 277: R140–R146, 1999.
24. **Niederhoffer N, Hein L, Starke K.** Modulation of the baroreceptor reflex by α_{2A}-adrenoceptors, a study in α_{2A} knockout mice. *Br J Pharmacol* 141: 851–859, 2004.
25. **Pelayo F, Dubocovich ML, Langer SZ.** Regulation of noradrenaline release in the rat pineal through a negative feedback mechanism mediated by presynaptic α-adrenoceptors. *Eur J Pharmacol* 45: 317–318, 1977.
26. **Philipp M, Brede M, Hein L.** Physiological significance of α_2-adrenergic receptor subtype diversity, one receptor is not enough. *Am J Physiol Regul Integr Comp Physiol* 283: R287–R295, 2002.
27. **Rump LC, Bohmann C, Schaible U, Schöllhorn J, Limberger N.** α2C-Adrenoceptor-modulated release of noradrenaline in human right atrium. *Br J Pharmacol* 116: 2617–2624, 1995.
27a. **Schwartz DD.** Activation of alpha-2 adrenergic receptors inhibits norepinephrine release by a pertussis toxin-insensitive pathway independent of changes in cytosolic calcium in cultured rat sympathetic neurons. *J Pharmacol Exp Ther* 282: 248–255, 1997.
28. **Sinclair MD.** A review of the physiological effects of α2-agonists related to the clinical use of medetomidine in small animal practice. *Can Vet J* 44: 885–897, 2003.
29. **Starke KM, Gothert M, Kilbinger H.** Modulation of neurotransmitter release by presynaptic autoreceptors. *Physiol Rev* 69: 864–989, 1989.
30. **Starke KM.** Presynaptic α-autoreceptors. *Rev Physiol Biochem Pharmacol* 107: 73–146, 1987.
31. **Starke K, Langer SZ.** A note on terminology for presynaptic receptors. In: *Presynaptic Receptors*, edited by Langer SZ, Starke K, and Dubocovich ML. Oxford, UK: Pergamon 1979, p. 1–3.
32. **Starke K, Endo T, Taube HD.** Pre- and post-synaptic components in effect of drugs with α-adrenoceptor affinity. *Nature* 254: 440–441, 1975.
33. **Starke K.** Alpha sympathomimetic inhibition of adrenergic and cholinergic transmission in the rabbit heart. *Naunyn Schmiedebergs Arch Pharmacol* 274: 18–45, 1972.
34. **Szabo B, Schramm A, Starke K.** Effect of yohimbine on renal sympathetic nerve activity and renal norepinephrine spillover in anesthetized rabbits. *J Pharmacol Exp Ther* 260: 780–788, 1992.
35. **Szabo B, Hedler L, Starke K.** Peripheral presynaptic and central effects of clonidine, yohimbine and rauwolscine on the sympathetic nervous system in rabbits. *Naunyn-Schmiedeberg's Arch Pharmacol* 340: 648–657, 1989.
37. **Vizi ES, Somogyi GT, Hadhazy P, Knoll J.** Effect of duration and frequency of stimulation on the presynaptic inhibition by α-adrenoceptor stimulation of the adrenergic transmission. *Naunyn-Schmiedeberg's Arch Pharmacol* 280: 79–91, 1973.
38. **Westfall TC.** Local regulation of adrenergic neurotransmission. *Physiol Rev* 57: 659–728, 1977.

Behavioral/Systems/Cognitive

Reverse of Age-Dependent Memory Impairment and Mitochondrial DNA Damage in Microglia by an Overexpression of Human Mitochondrial Transcription Factor A in Mice

Yoshinori Hayashi,[1]* Masayoshi Yoshida,[2,4]* Mayumi Yamato,[3]* Tomomi Ide,[2] Zhou Wu,[1] Mayumi Ochi-Shindou,[1] Tomotake Kanki,[4] Dongchon Kang,[4] Kenji Sunagawa,[2] Hiroyuki Tsutsui,[5] and Hiroshi Nakanishi[1]

[1]Laboratory of Oral Aging Science, Faculty of Dental Sciences, [2]Department of Cardiovascular Medicine, Graduate School of Medical Sciences, [3]Department of REDOX Medicinal Science, Graduate School of Pharmaceutical Sciences, [4]Department of Clinical Chemistry and Laboratory Medicine, Kyushu University, Fukuoka 812-8582, Japan, and [5]Department of Cardiovascular Medicine, Hokkaido University Graduate School of Medicine, Sapporo 060-8638, Japan

Mitochondrial DNA (mtDNA) is highly susceptible to injury induced by reactive oxygen species (ROS). During aging, mutations of mtDNA accumulate to induce dysfunction of the respiratory chain, resulting in the enhanced ROS production. Therefore, age-dependent memory impairment may result from oxidative stress derived from the respiratory chain. Mitochondrial transcription factor A (TFAM) is now known to have roles not only in the replication of mtDNA but also its maintenance. We herein report that an overexpression of TFAM in HeLa cells significantly inhibited rotenone-induced mitochondrial ROS generation and the subsequent NF-κB (nuclear factor-κB) nuclear translocation. Furthermore, TFAM transgenic (TG) mice exhibited a prominent amelioration of an age-dependent accumulation of lipid peroxidation products and a decline in the activities of complexes I and IV in the brain. In the aged TG mice, deficits of the motor learning memory, the working memory, and the hippocampal long-term potentiation (LTP) were also significantly improved. The expression level of interleukin-1β (IL-1β) and mtDNA damages, which were predominantly found in microglia, significantly decreased in the aged TG mice. The IL-1β amount markedly increased in the brain of the TG mice after treatment with lipopolysaccharide (LPS), whereas its mean amount was significantly lower than that of the LPS-treated aged wild-type mice. At the same time, an increased mtDNA damage in microglia and an impaired hippocampal LTP were also observed in the LPS-treated aged TG mice. Together, an overexpression of TFAM is therefore considered to ameliorate age-dependent impairment of the brain functions through the prevention of oxidative stress and mitochondrial dysfunctions in microglia.

Key words: mitochondria DNA; transcription factor A; oxidative stress; aging; memory impairment; microglia

Introduction

It is widely believed that oxidative stress and inflammation are major causative factors for a progressive decline in motor and memory functions during aging in humans and animals (Forster et al., 1996; Navarro et al., 2002). Behavioral dysfunctions associated with aging are also postulated to be associated with a decreased activity of mitochondrial electron transfer complexes with aging (Navarro et al., 2004, 2005). Furthermore, increased intracellular reactive oxygen species (ROS) activate microglia, which are representative resident mononuclear phagocyte populations in the brain, to induce an increased production of inflammatory mediators (Pawate et al., 2004; Qin et al., 2005). ROS generated in close proximity and in large concentrations by the mitochondrial respiratory chain cause oxidation of unsaturated fatty acid, proteins, and DNA. Mitochondrial DNA (mtDNA) is highly susceptible to damage produced by ROS because of its close proximity to ROS generation through the respiratory chain and its paucity of protective histones. Furthermore, there is little capacity for DNA repair in the mitochondria. During aging, a large number of mtDNA mutations accumulate in various tissues including the brain, thus leading to dysfunction of the respiratory

Received March 3, 2008; revised July 7, 2008; accepted July 15, 2008.

This work was supported by Grants-in-Aid for Scientific Research and Grant-in-Aid for Scientific Research on Priority Area from the Ministry for Education, Science, and Culture, Japan; a Labor Science Research Grant for Comprehensive Research in Aging and Health Labor and Welfare of Japan; and the Uehara Research Foundation. We thank Prof. V. Hugh Perry (CNS Inflammation Group, School of Biological Sciences, University of Southampton, Southampton, UK) for his critical reading of this manuscript. We also thank Keiko Kurakazu for technical assistance and Drs. Atsushi Fukuoh and Kippei Ohgaki for technical advice.

*Y.H., M. Yoshida, and M. Yamato contributed equally to this work.

Correspondence should be addressed to either of the following: Dr. Tomomi Ide, Department of Cardiovascular Medicine, Kyushu University Graduate School of Medicine, 3-1-1, Maidashi, Higashi-ku, Fukuoka 812-8582, Japan, E-mail: tomomi_i@cardiol.med.kyushu-u.ac.jp; or Dr. Hiroshi Nakanishi, Laboratory of Oral Aging Science, Faculty of Dental Sciences, Kyushu University, 3-1-1, Maidashi, Higashi-ku, Fukuoka 812-8582, Japan, E-mail: nakan@dent.kyushu-u.ac.jp.

M. Ochi-Shindou's present address: Neurobiology Research Unit, Okinawa Institute of Science and Technology, Okinawa 904-2234, Japan.

DOI:10.1523/JNEUROSCI.1957-08.2008

 0270-6474/08/288624-11$15.00/0

chain. Finally, deficits in the respiratory chain result in the enhanced ROS production, culminating in age-dependent memory impairments (Corral-Debrinski et al., 1992; Lin et al., 2002). Therefore, the vulnerability of mtDNA to ROS is a major determinant factor for deficits in the brain functions in aging.

Mitochondrial transcription factor A (TFAM) is a nucleus-encoded protein that binds upstream of the light-strand and heat-strand promoters of mtDNA and promotes the transcription of mtDNA (Parisi and Clayton, 1991). Moreover, there is increasing evidence that TFAM plays an important role in maintaining mtDNA and regulating its copy number. The amount of mtDNA is closely correlated with the amount of TFAM but not with the transcription level, and the majority of TFAM molecules are involved in architecturally maintaining the higher structure of mtDNA (Kanki et al., 2004b). More recently, transgenic mice that overexpressed human TFAM under control of the β-actin promoter were generated and showed an increased copy number of mtDNA in the myocardium and the protection of the heart from mitochondrial dysfunction (Ikeuchi et al., 2005). The improvement in mitochondrial respiratory function may thus lead to an amelioration of the chronic process of remodeling by decreasing the mitochondrial ROS generation. The brain has a higher demand for oxygen; therefore, it is possible that increased oxidative stress and consequent mtDNA mutations may lead to the accumulation of lipid peroxidation products. Furthermore, it is reasonable to speculate that such TFAM overexpression may also inhibit the mitochondrial ROS generation through a reduction of the mtDNA mutations, which may retard the motor and memory functions.

To address this issue, the effects of TFAM overexpression on age-dependent deficits in brain functions were examined using human TFAM transgenic (TG) mice. The present study showed a significant improvement in the age-dependent memory impairments in TG mice because of a marked reduction in both oxidative stress and inflammation in the brain.

Materials and Methods

All experimental procedures of this study were approved by the Animal Care and Use Committee of Kyushu University.

Overexpression of TFAM in HeLa cells using the tetracycline-regulation system. Tetracycline-regulated TFAM-overexpressing cell lines were produced as previously reported (Parisi and Clayton, 1991). The cells were grown in DMEM containing 10% fetal bovine serum, 400 mg/ml Geneticin (G418), and 200 mg/ml hygromycin B, with or without 1 mg/ml doxycycline (DC) and maintained at 37°C in humidified air with 5% CO_2. The cells were then seeded in 24-well dishes and the culture medium was replaced after 24 h with serum-free DMEM containing 400 mg/ml G418 and 200 mg/ml hygromycin B, with or without 1 mg/ml DC. After 24 h, the cells were treated for 6 h with 0.001% of 1 mol/L rotenone dissolved in ethanol. The protein levels of human TFAM in the soluble fractions of HeLa cells in the presence and absence of DC were analyzed by immunoblotting.

Rotenone-induced ROS measurement. Intracellular ROS was measured by a ROS-sensitive fluorescent probe, 2,7-diamino-10-ethyl-9-phenyl-9,10-dihydrophenanthridine (DHE), in tetracycline-regulated HeLa cells. The cells were plated in 96-well culture dishes and cultured for 24 h at 37°C in humidified air with 5% CO_2, followed by incubation in serum-free medium for another 24 h. Next, the cells were treated with 1 μmol/L rotenone for 5.5 h and then with 2 μmol/L DHE for 30 min. The fluorescent intensity was determined immediately at excitation wavelength of 485 nm and emission wavelength of 530 nm on a fluorescent plate reader. The cellular images for DHE oxidation were observed using confocal laser-scanning microscope (CLSM) (LSM510MET; Carl Zeiss).

CLSM images for nuclear factor-κB nuclear translocation. Tetracycline-regulated TFAM-overexpressing HeLa cells were seeded in 24-well dish at a density of 10^3 cells/mm^2. The culture medium was replaced after 24 h with serum-free DMEM medium containing 400 mg/ml G418 and 200 mg/ml hygromycin B, with or without 1 mg/ml DC. After 24 h, the cells were treated for 6 h with 0.001% (final concentration in medium) of 1 mol/L rotenone dissolved in ethanol. After treatment with rotenone or vehicle, the cells were fixed with 4% paraformaldehyde and then incubated with mouse anti-p65 monoclonal antibody (Santa Cruz Biotechnology; AH Diagnostics) in bovine serum albumin (BSA)/PBS overnight at 4°C, washed three times with PBS, and then incubated with a secondary Alexa 488 goat anti-mouse IgG antibody in BSA/PBS for 1 h at room temperature. After three washes, the nuclei of cells were counterstained with propidium iodide (Sigma-Aldrich). The cells showing bright staining for p65 in the nucleus were scored, and the results were presented as a percentage of the number of cells with nuclear factor-κB (NF-κB) nuclear translocation to the total number of cells examined.

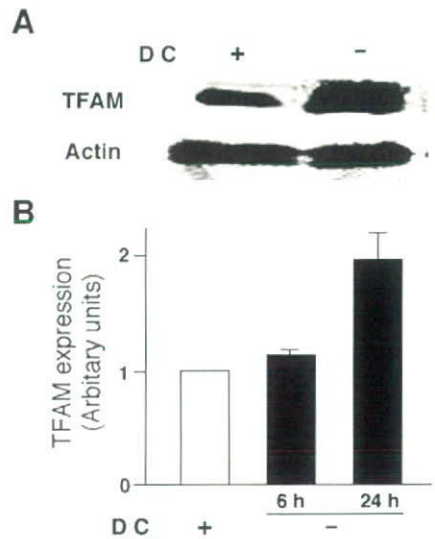

Figure 1. Protein levels of human TFAM overexpressed by the tetracycline-off system in HeLa cells. ***A***, Immunoblot analysis of human TFAM expressed in HeLa cells cultured with and without DC for 24 h. ***B***, The mean protein level of human TFAM in HeLa cells cultured with and without DC for 6 and 24 h. The mean relative immunoreactivity of each protein band was determined using the level of actin as an internal control. Each column and bar represent the mean and SEM of three experiments, respectively.

Animals. The methods for generating TG mice that overexpressed human TFAM has been described previously (Ikeuchi et al., 2005). The animals were housed under 12 h light/dark cycle (lights on at 8:00 A.M.) with access to food and water *ad libitum*. All mice were handled daily for 5 d before the start of the experiment to minimize stress reactions to manipulation.

Immunoblotting. Antibodies against human TFAM and mouse Tfam were produced by immunizing rabbits with recombinant glutathione *S*-transferase-tagged human TFAM and mouse Tfam. The protein levels of human TFAM and mouse endogenous TFAM were analyzed in the soluble fractions of brain tissue homogenates as previously described (Lin et al., 2002).

Thiobarbituric acid reactive substances. Twenty male C57BL/6 mice [wild type (WT) and TG] of the following age groups: young (2 months of age; WT, $n = 5$; TG, $n = 5$) and aged (24 months of age; WT, $n = 5$; TG, $n = 5$) were used for the measurement of thiobarbituric acid reactive substances (TBARS). The homogenates of whole brains were mixed with 0.4% SDS, 7.5% acetic acid adjusted to pH 3.5 with NaOH, and 0.3% thiobarbituric acid. The mixture was kept at 5°C for 60 min and then heated at 100°C for 60 min. After cooling, the mixture was extracted with distilled water and *n*-butanol:pyridine (15:1, v/v) and centrifuged at 16,000× *g* for 10 min. The fluorescence of the supernatant was measured at excitation and emission wavelengths of 510 and 550 nm, respectively, using GENios Pro (Tecan). The standard was prepared using TEP (1,1,3,3-tetraethoxypropane).

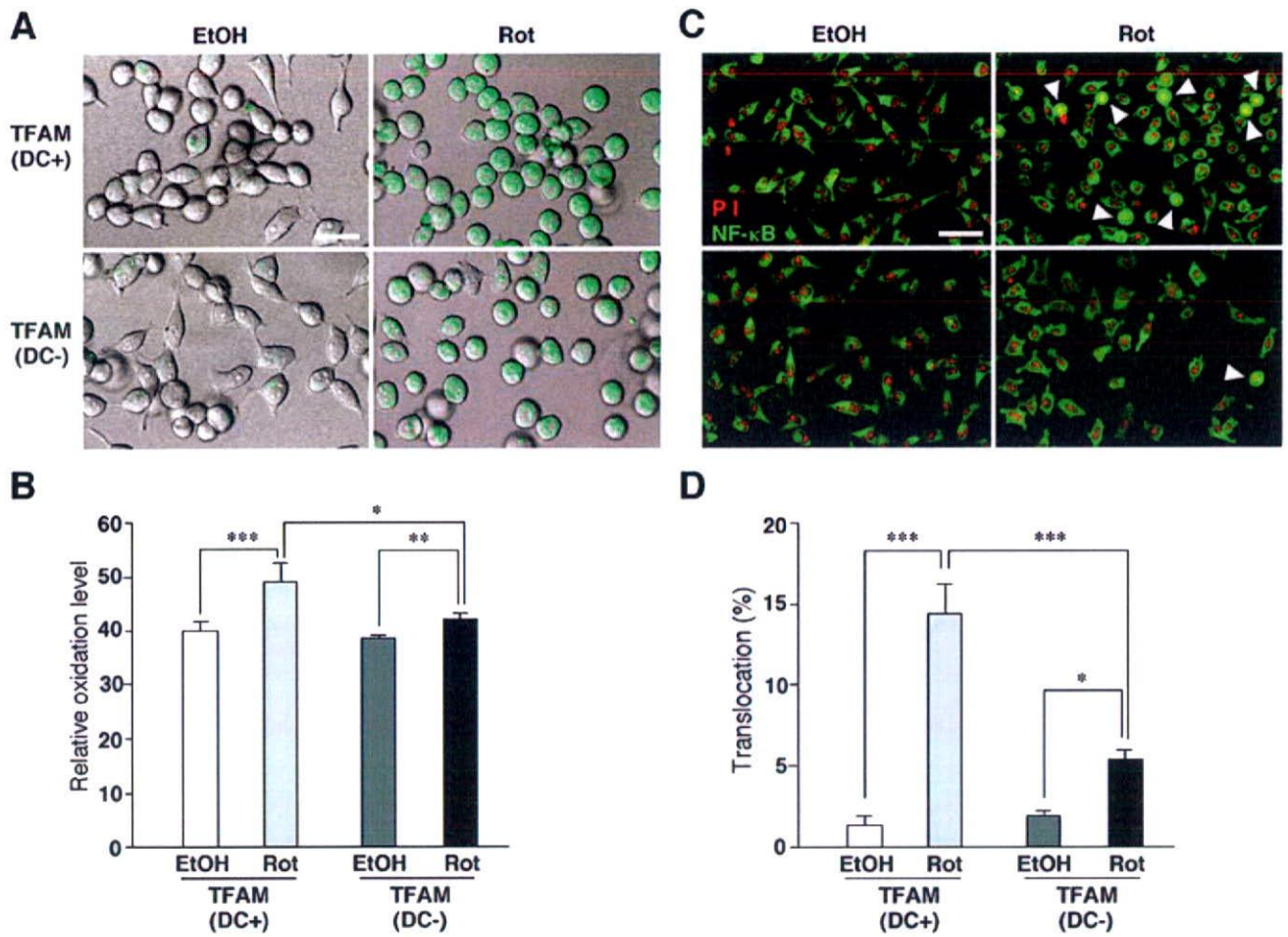

Figure 2. Effects of an overexpression of TFAM by the tetracycline-off system on rotenone-induced intracellular ROS generation and NF-κB nuclear translocation in HeLa cells. ***A***, CLMS images of rotenone-induced intracellular ROS generation measured using a ROS-sensitive dye (green), DHE, in HeLa cells cultured with or without DC. Scale bar, 20 μm. ***B***, The mean DHE oxidation levels in HeLa cells cultured with or without DC after treatment with EtOH or rotenone. Each column and bar represent the mean ± SEM of six experiments. The asterisks indicate a significant difference between two groups (*$p < 0.05$; **$p < 0.01$; ***$p < 0.001$). ***C***, NF-κB (green) and propidium iodide (PI)-stained nuclei (red) in HeLa cells cultured with or without DC after the treatment with EtOH or rotenone. The arrowheads show HeLa cells with the nuclear translocated NF-κB. Scale bar, 50 μm. ***D***, The mean percentage of the NF-κB nuclear translocation in HeLa cells cultured with or without DC after the treatment with EtOH or rotenone. Each column and bar represent the mean ± SEM of nine experiments. The asterisks indicate significant differences between two groups (*$p < 0.05$; ***$p < 0.001$). Rot, Rotenone.

Mitochondrial enzyme activities. Twenty male C57BL/6 mice (WT and TG) of the following age groups: young (2 months of age; WT, $n = 5$; TG, $n = 5$) and aged (24 months of age; WT, $n = 5$; TG, $n = 5$) were used to measure the mitochondrial enzyme activities. The specific activity of mitochondrial complex enzymes, including complexes I, II, III, and IV, was measured in mitochondria isolated from whole brains of each group as described previously (Ide et al., 1999). The specific activity of rotenone-sensitive NADH-ubiquinone oxidoreductase (complex I) was measured by reduction of the ubiquinone analog decylubiquinone. For the activity of succinate ubiquinone oxidoreductase (complex II), the reduction of 2,6-dichlorophenolindophenol when coupled to complex II-catalyzed reduction of decylubiquinone was measured. For the specific activity of ubiquinol/cytochrome *c* oxidoreductase (complex III), the reduction of cytochrome *c* catalyzed by complex III in the presence of reduced decylubiquinone was monitored. The specific activity of cytochrome *c* oxidase (complex IV) was measured by following the oxidation of reduced cytochrome *c*, which was prepared in the presence of dithionite. All enzymatic activities were expressed as nanomoles per minute per milligram of protein.

Immunohistochemistry. Twenty-four male C57BL/6 mice (WT and TG) of the following age groups: young (2–4 months of age; WT, $n = 6$; TG, $n = 6$) and aged (20–24 months of age; WT, $n = 6$; TG, $n = 6$) were used for the immunohistochemical analyses. WT and TG mice of both young and aged groups were anesthetized with sodium pentobarbital (40 mg/kg, i.p.) and killed by intracardiac perfusion with isotonic saline followed by PBS, pH 7.4. After perfusion, the brain was removed and further fixed by immersion in 4% paraformaldehyde overnight at 4°C, and then immersed in 30% sucrose for 24 h at 4°C. Floating coronal sections (10 μm thick) of the hippocampus were prepared by a cryostat and stained with anti-human TFAM, anti-8-oxo-deoxyguanosine (8-oxo-dG) (NOF Corporation), anti-4-hydroxy-2-nonenal (HNE) (Alpha Diagnostic), and anti-interleukin-1β (IL-1β) (Santa Cruz Biotechnology) for 3 d at 4°C. To detect any oxidative damage in the mitochondrial DNA rather than in the nuclear DNA, the sections were directly treated with anti-8-oxo-dG antibody without treatment of HCl as described previously (Kajitani et al., 2006). After washing with PBS, the sections were stained using the avidin–biotin–peroxidase complex method (Vector Laboratories). After washing with PBS, the sections were reacted with 0.015% 3′,3-diaminobenzidine/0.4% $(NH_4)_2Ni(SO_4)_2$/0.09% H_2O_2/0.1 mol/L Tris-buffered saline for 5–10 min. The sections were rinsed thoroughly with PBS, mounted, and coverslipped. As negative controls, the sections were incubated with nonimmune rabbit IgG or mouse IgG instead of the first antibody and processed in the same manner as described above.

For double fluorescent staining, the floating sections were stained with the following combinations of the first antibodies for 48 h at 4°C: anti-

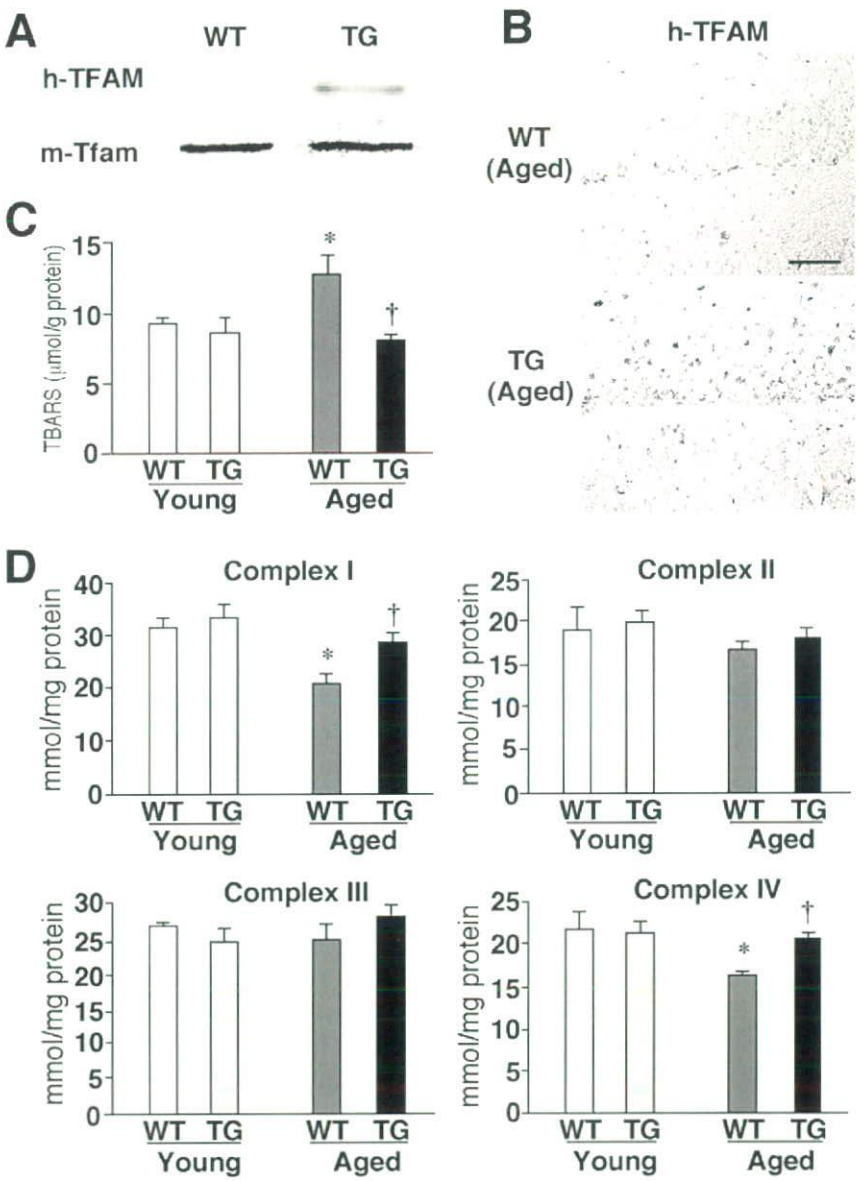

Figure 3. The effects of TFAM overexpression on age-dependent increased oxidative stress in the brain. ***A***, Expression of TFAM in the brain. Immunoblotting was performed using specific antibodies against human TFAM (h-TFAM) and mouse Tfam (m-Tfam) in soluble brain extracts prepared from the young WT and TG mice. ***B***, Immunohistochemical staining for H-TFAM in the CA1 hippocampal subfield of aged WT and TG mice. Scale bar, 50 μm. ***C***, The mean lipid peroxidation levels measured using a biochemical assay for TBARS in the brain tissues prepared from the WT and TG mice of both age groups. Each column and bar represent the mean ± SEM of five experiments. An asterisk indicates a significant difference versus the young WT mice ($^*p < 0.05$). A dagger indicates a significant difference versus the aged WT mice ($^\dagger p < 0.05$). ***D***, The mean activity of mitochondrial respiratory enzymes, complexes I to IV, in brain tissues prepared from the WT and TG mice of both age groups. Each column and bar represent the mean ± SEM of five experiments. The asterisks indicate significant differences versus the young WT mice ($^*p < 0.05$). The daggers indicate significant differences versus the aged WT mice ($^\dagger p < 0.05$).

8-oxo-dG and anti-Iba1 IgGs (Wako Pure Chemicals Industries); anti-8-oxo-dG and anti-GFAP IgGs (Sigma-Aldrich); anti-8-oxo-dG and anti-MAP2 IgGs (Millipore Bioscience Research Reagents); anti-HNE IgG and F4/80 (Serotec); anti-HNE and anti-GFAP IgGs; anti-HNE and anti-NeuN IgGs (Millipore Bioscience Research Reagents); anti-IL-1β and anti-Iba1 IgGs; anti-IL-1β and anti-GFAP IgGs; anti-IL-1β and anti-NeuN IgGs; 8-oxo-dG and anti-cytochrome *b* (Cyt *b*) IgGs (Kanki et al., 2004b). After washing with PBS, the sections were incubated with a mixture of 0.5% Alexa 488 anti-mouse IgG and Cy3 anti-rabbit IgG, 0.5% Alexa 488 anti-rabbit IgG and Cy3 anti-mouse IgG (GE Healthcare) for 2 h at room temperature. Some sections immunostained using anti-8-oxo-dG and anti-HNE IgGs were stained with an RNA/DNA marker, YOYO-1 (Invitrogen). After several washes with PBS, the sections were mounted in the antifading medium Vectashield (Vector Laboratories) and examined with a CLSM (LSM510MET; Carl Zeiss). To quantitatively assess the immunofluorescence intensity of IL-1β in microglia, the immunofluorescence intensity of IL-1β within Iba1-positive cells was measured as the average pixel intensity. The immunofluorescence intensity of 8-oxo-dG within Cyt *b*-positive mitochondria was also measured as the average pixel intensity.

Behavioral tests. Twenty-four male C57BL/6 mice (WT and TG) of the following age groups: young (2 months of age; WT, $n = 6$; TG, $n = 6$) and aged (24 months of age; WT, $n = 6$; TG, $n = 6$) were used in the following behavioral tests.

For the cylinder test, the modified cylinder test was used to monitor locomotor activity in a novel environment (Tillerson et al., 2002). In short, each animal was placed in a glass cylinder (diameter, 10 cm; height, 14 cm) and was videotaped for 6 min. The mice responded to the novel environment by standing on their hindlimbs and leaning on the walls of the cylinder with their forelimbs. The number of supporting paw placements performed independently with the left and the right paws were counted for the first 3 min. The forelimb use score was described by expressing the total number of wall contacts performed with both forelimbs.

For the measurement of locomotor activities, mice were removed from their home cages and placed in a novel home cage (clean and without bedding), which provided a floor area of 28 × 18 cm, and then the locomotor activity of mice of each genotype and each different age group was scored for 3 min. The novel home cage was divided into six identical rectangles and a trained observer determined the incidence of line crossing.

For the rotarod test, an automated single lane rotarod treadmill (Muromachi; 3 cm diameter drums with grooves to improve the grip) that could be set at either a fixed speed or an accelerating speed was used. For the fixed speed rotarod protocol, all mice were pretrained on the rotarod apparatus in order for them to reach a stable performance as described by Iancu et al. (2005). The training consisted of three sessions on 2 consecutive days, whereby each session included three separate test trials, each lasting 120 s. The mice were trained at 5, 10, and 15 rpm. On day 1, mice were trained at 5 rpm. On day 2, mice were trained once in the morning at 10 rpm and once again in the afternoon at 15 rpm. The final test (three sessions, each lasting 180 s) was performed on the third day at 15 rpm. For each trial, the mouse was gently placed on the stopped rod, with its body axis perpendicular to the rotation axis and the head oriented to the same direction of rotation, so that the animal had to turn their position against the direction of rotation and progress forward to avoid a fall from the rod after the rod started to rotate. Between trials, the mice were given at least 10 min of rest to reduce stress and fatigue. The length of time that each animal was able to stay on the rod was recorded as the latency to fall, and it was registered automatically by a trip switch under the floor of the rotating drum.

For the radial maze test, an apparatus was created as described previ-